

This is the peer reviewed version of the following article: Lucas, S. J., Michel, C. B., Marra, V. , Smalley, J. L., Hennig, M. H., Graham, B. P. and Forsythe, I. D. (2018), Glucose and lactate as metabolic constraints on presynaptic transmission at an excitatory synapse. *Journal of Physiology*, 596: 1699-1721, which has been published in final form at <https://doi.org/10.1113/JP275107>. This article may be used for non-commercial purposes in accordance With Wiley Terms and Conditions for self-archiving.

1 Glucose and lactate as metabolic constraints on presynaptic
2 transmission at an excitatory synapse

3
4 Running title: Energy constraints on presynaptic function

5
6 Sarah J. Lucas¹, Christophe B. Michel², Vincenzo Marra¹, Joshua L. Smalley¹,
7 Matthias H. Hennig³, Bruce P. Graham² & Ian D. Forsythe^{1*}.

8 ¹ Department of Neuroscience, Psychology & Behaviour, University of Leicester,
9 Leicester, LE1 9HN, UK.

10 ² Computing Science & Mathematics, Faculty of Natural Sciences, University of
11 Stirling, Stirling, FK9 4LA, UK.

12 ³ Institute for Adaptive and Neural Computation, School of Informatics, University of
13 Edinburgh, Edinburgh, EH8 9AB, UK.

14
15 * Corresponding author, e-mail: idf@le.ac.uk

16 Number of figures: 12

17 Number of tables: 1

18
19 The authors declare no competing financial interests

20 **Acknowledgements**

21 This research was supported by the Biotechnology and Biological Sciences
22 Research Council (IDF, MHH, BPG) and the Wellcome Trust (VM).

23 JLS present address: Department of Neuroscience, Tufts University School of
24 Medicine, Boston, MA 02111, USA.

Abstract

The synapse has high energy demands, which increase during intense activity. Presynaptic ATP production depends on substrate availability and usage will increase during activity, which in turn could influence transmitter release and information transmission. We investigated transmitter release at the mouse calyx of Held synapse using glucose or lactate (10, 1 or 0 mM) as the extracellular substrates while inducing metabolic stress. High frequency stimulation (HFS) and recovery paradigms evoked trains of EPSCs monitored under voltage-clamp. Whilst postsynaptic intracellular ATP was stabilised by diffusion from the patch pipette, depletion of glucose increased EPSC depression during HFS and impaired subsequent recovery. Computational modelling of these data demonstrated a reduction in the number of functional release sites and slowed vesicle pool replenishment during metabolic stress, with little change in release probability. Directly depleting presynaptic terminal ATP impaired transmitter release in an analogous manner to glucose depletion. In the absence of glucose, presynaptic terminal metabolism could utilise lactate from the aCSF and this was blocked by inhibition of monocarboxylate transporters (MCT). MCT inhibitors significantly suppressed transmission in low glucose, implying that lactate is a presynaptic substrate. Additionally, block of glycogenolysis accelerated synaptic transmission failure in the absence of extracellular glucose, consistent with supplemental supply of lactate by local astrocytes. We conclude that both glucose and lactate support presynaptic metabolism and that limited availability, exacerbated by high intensity firing, constrains presynaptic ATP, impeding transmission through a reduction in functional presynaptic release sites as vesicle recycling slows when ATP levels are low.

51

52 **Key Points**

- 53 • Synapses have high energy demands which increase during intense activity.
54 We show that presynaptic terminals can utilize extracellular glucose or lactate
55 to generate energy to maintain synaptic transmission.
- 56 • Reducing energy substrates induces a metabolic stress: presynaptic ATP
57 depletion impaired synaptic transmission through a reduction in the number of
58 functional synaptic vesicle release sites and a slowing of vesicle pool
59 replenishment, without a consistent change in release probability.
- 60 • Metabolic function is compromised in many pathological conditions (e.g.
61 stroke, traumatic brain injury and neurodegeneration). Knowledge of how
62 synaptic transmission is constrained by metabolic stress, especially during
63 intense brain activity will provide insights to improve cognition following
64 pathological insults.

65

66

67 **Introduction**

68 Energy provision for synaptic transmission is crucial for cognition and the
69 relationship between brain activity and local nutrient supply is exploited in fMRI
70 imaging. Transmission of information across synapses requires high levels of energy
71 to maintain ionic gradients, Ca^{2+} extrusion and vesicular recycling (Attwell and
72 Laughlin, 2001; Harris et al., 2012), hence during periods of high activity an
73 imbalance between energy generation and consumption may influence neuronal
74 function and compromise information transmission. The study of neuronal
75 metabolism is often based on primary cultures and pharmacological block of

glycolysis or mitochondrial respiration; but to understand energy constraints on information transmission a more physiological situation would be advantageous.

Metabolic demand is not uniform and varies between brain regions, with the auditory pathway having some of the highest metabolic rates in the nervous system (Sokoloff et al., 1977). The calyx of Held/MNTB synapse in the auditory brainstem can sustain high frequency transmission at rates of over 300 Hz (Kopp-Scheinpflug et al., 2011). The density, proximity, and morphology of mitochondria close to the presynaptic active zone is consistent with high metabolic rates at the calyx of Held (Satzler et al., 2002; Perkins et al., 2010). The large size of the calyx presynaptic terminal and its target onto single neurons in the medial nucleus of the trapezoid body (MNTB) allows access to both the pre- and postsynaptic compartments and makes it an ideal preparation for direct investigation of metabolic influence (see von Gersdorff & Borst, 2002; Schneggenburger & Forsythe 2006).

Glucose deprivation is well known to compromise synaptic transmission (Akasu et al., 1996; Calabresi et al., 1997; Izumi et al., 1997). The mechanisms through which energy depletion impairs presynaptic function are the subject of intense interest in terms of both basic science and the association with diabetes, aging and dementia (Duarte, 2015; Feinkohl et al., 2014). The brain as a whole, preferentially metabolises glucose to meet its energy demands, but the extent to which neurons use glucose directly and/or require lactate via the astrocyte-neuron lactate shuttle (ANLS) (Pellerin and Magistretti, 1994) is a matter of debate. Some recent studies have indicated that the lactate shuttle is required to maintain neuronal function (Nagase et al., 2014; Suzuki et al., 2011), while others have proposed that glucose is the primary neuronal energy source (Dienel, 2012; Simpson et al., 2007).

We have used the calyx of Held/MNTB synapse in an *in vitro* brain slice preparation to measure the contribution of energy substrates, glucose and lactate, in maintaining synaptic transmission. This configuration allows recording from both the presynaptic calyx and postsynaptic neuron, and also preserves the close association of a supporting glial cell with the synapse (Uwechue et al., 2012). The results show that at physiological concentrations, glucose was used directly by the terminal, but that lactate also contributed to the maintenance of normal synaptic transmission. Glucose depletion increased synaptic depression during high frequency stimulation (HFS) and impaired the subsequent recovery of EPSC amplitude. This effect of glucose depletion was mimicked by dialysing the presynaptic terminal with low ATP (0.1 mM). Model-based analysis of the experimental data indicated that impairment in ATP availability causes a significantly greater decline in the size of the readily releasable vesicle pool (RRVP), with the RRVP failing to recover even after minutes of rest between HFS epochs. This suggests that the metabolic demand of vesicle recycling places constraints on synaptic function under metabolic stress.

Materials and Methods

Electrophysiology & live fluorescent imaging

Experiments were performed in accordance with the Animals (Scientific Procedures) Act 1986, UK. Transverse brainstem slices (thickness: 250 μ m for postsynaptic recording with synaptic stimulation and 120 μ m for paired pre- and post-synaptic recordings) were prepared from male and female P13-18 CBA/Ca mice killed by decapitation. Slices containing the MNTB were prepared in an ice-cold high sucrose saline composed of (in mM); sucrose (250), KCl (2.5), NaHCO₃ (26), NaH₂PO₄

(1.25), D-glucose (10), ascorbic acid (0.5), MgCl_2 (4) and CaCl_2 (0.1) saturated with 95% O_2 and 5% CO_2 . Slices recovered in oxygenated artificial cerebrospinal fluid (aCSF) for at least 1 h at 34 °C. The aCSF was composed of (in mM); NaCl (125), NaHCO_3 (26), KCl (2.5), NaH_2PO_4 (1.25), myo-inositol (3), D-glucose (10), MgCl_2 (1), and CaCl_2 (2).

Whole-cell patch recordings were made from single slices held in a recording chamber at 33 ± 2 °C and perfused at 1 ml/min with oxygenated aCSF. We performed either postsynaptic recordings, or paired recordings where we simultaneously patched both the presynaptic terminal and postsynaptic neuron. Glass recording pipettes had a resistance of 3-6 M Ω . Postsynaptic pipettes were filled with a whole-cell patch solution composed of (in mM) K-gluconate (97.5), KCl (32.5), HEPES (5), EGTA (5), NaCl (5), MgCl_2 (1) and $\text{K}_2\text{-ATP}$ (2); presynaptic pipettes contained (in mM) K-gluconate (97.5), KCl (32.5), HEPES (10), EGTA (0.2), MgCl_2 (1), Na-glutamate (10), Na-GTP (0.3). Stated voltages were not corrected for a liquid junction potential of -9 mV.

Chemicals and drugs were purchased from Sigma-Aldrich unless specified. Other drugs were purchased as listed here: monocarboxylate transporter inhibitor AR-C155858 (Tocris, 4960) FM1-43FX (Molecular Probes, cat. no. F35355) alpha-Latrotoxin (Alomone, LSP-130) Bromophenol Blue (Acros, cat. no. 151340250). Drugs were applied by perfusion in the aCSF.

MNTB neurons with calyceal inputs were visually identified using a Nikon Eclipse E600FN and a 60x DIC objective. Recordings were made using a Multiclamp 700B

amplifier and Clampex/Clampfit software (Molecular Devices) for data acquisition and analysis. Responses were digitised at 20 kHz and filtered at 10 kHz, and the whole-cell capacitance compensated. The mean series resistance was 16 MOhms (range 6-25 MOhms) and series resistance was compensated by 70 %. Experiments were interleaved between control and test conditions through the experiments and the Rs were similar for each data set. Rs was checked prior to each 30s train and after the last recovery stimulation of each epoch throughout the 20-35 minutes of recording. Recordings discarded if the series resistance changed by more than 20 %, or went above 25 MOhms. EPSCs were recorded from MNTB neurons voltage-clamped at a holding potential of -40 mV. A bipolar stimulating electrode was positioned at the midline to evoke action potentials in the axons projecting to the MNTB; high frequency stimulation (HFS; 100 Hz for 30s) was given, followed by 6 pulses over the subsequent 30s to probe the recovery (Figure 1B). This protocol was given 10 min after a change in the aCSF composition and then repeated at 5 min intervals (i.e. at 15, 20, 25 and 30 mins) in all unpaired experiments (see example in Figure 1 E & F). The stimulation voltage was twice the voltage threshold required to evoke an EPSC. Presynaptic terminals were voltage-clamped at -80 mV and HFS (100 Hz for 2 s) and subsequent recovery pulses evoked using voltage ramps to mimic action potentials (Figure 5A). The HFS protocol was given 1-2 min after breaking into the presynaptic terminal and then repeated 5 min later. The peak EPSC was mediated by AMPAR, with little contribution from NMDAR at this age and potential (Steinert et al., 2010). AMPAR desensitization also had little or no impact on synaptic response amplitude at near physiological temperatures and with 10 ms between stimuli (Wong et al., 2003).

Live imaging of slices was performed with slices perfused with aCSF containing 10 mM glucose or zero glucose and with a stimulating electrode placed at the midline to give 4x HFS at 5 min intervals. FM1-43FX dye (10 μ M) was applied 1 minute before the third (20 min) HFS and was present until 1 minute after the end of the stimulation to allow endocytosis of released vesicles and subsequent internalization of FM1-43FX. Bromophenol Blue (BPB, 0.5 mM, Harata et al., 2006) was then perfused in the extracellular solution to quench residual FM-143FX fluorescence. Live imaging was performed at 2 Hz, immediately before and during the fourth (25 min) HFS using a Nikon water immersion objective (40x, NA 0.8), a Nikon HGFI mercury lamp, a 470/40nm excitation filter, a 630/60nm emission filter and an Optimos sCMOS camera (Q-Imaging) controlled via Micro-Manager software (RRID:SCR_000415; Edelstein et al., 2014). Following the fourth HFS, α -Latrotoxin (Lat, 10 nM) was applied for 2 minutes to deplete the releasable pool before acquisition of a final image. Fluorescence values in Lat were used to normalise the total vesicular fluorescence, and fluorescence was quantified using Fiji (RRID:SCR_002285; Schindelin et al., 2012) terminals were analysed only if the rate of fluorescence loss was 5 times faster than photobleach measured at background regions.

Analysis

Prism software (RRID:SCR_002798) was used to fit the recovery curves to mean data, to perform t-tests, two-way ANOVA or two-way repeated measures (RM) ANOVAs (followed by Dunnett's or Bonferroni post hoc tests, as appropriate). For 30 s trains every 100th EPSC was analysed, and for the 2 s trains every 10th EPSC was analysed by two-way RM-ANOVA, due to the large number of EPSCs. Data are mean \pm SEM with statistical confidence <0.05 (α , presented as p, specific values). A

power calculation ($1-\beta$, %) for statistical significant data indicates the probability that type II errors have been excluded (<http://clincalc.com/stats/power.aspx>). Sample size, n , is the number of electrophysiology recordings; all were from different animals except for the paired recordings, where the number of animals used is given in brackets. For imaging experiments n is the number of calyces.

Western blot

Protein immunoblots were conducted using standard methods. Briefly, tissue samples were homogenised using a pestle homogeniser in RIPA buffer (150 mM sodium chloride, 1 % Triton X-100, 0.5 % sodium deoxycholate, 0.1 % SDS and 50 mM Tris, pH 8.0) supplemented with Mini cOmplete and PhosStop protease and phosphatase inhibitors. The resulting solution was sonicated and the protein concentration measured using a Bradford assay. 50 mg of total protein lysate was subjected to SDS-PAGE electrophoresis. Subsequently, proteins were transferred to nitrocellulose membrane and protein bands visualised in a FujiFilm LAS-3000 imager using primary antibodies, HRP-conjugated secondary antibodies and ECL reagents (Pierce, UK).

Modelling

A mathematical model of the EPSC amplitude in response to presynaptic action potentials (APs) at the calyx of Held was developed from a previously published model based on extensive experimental data (Meyer et al., 2001; von Gersdorff & Borst, 2002; Hennig et al., 2008). New model components are added to account for the effects of ATP depletion. All model components are described as follows.

224 The fraction of transmitter, T , released from the presynaptic terminal in response to a
 225 single AP arriving at time t , depends on the readily releasable vesicle pool (RRVP)
 226 occupancy, n , and the vesicle release probability, p :

$$T(t) = n(t).p(t)$$

227 Both the release probability and vesicle pool size are dynamic variables, allowing
 228 modelling of vesicle pool depletion, and facilitation and slow depression of release
 229 probability (Hennig et al., 2008). EPSC amplitude is assumed to be proportional to T .

230 The RRVP size is modelled as a continuous normalised variable, $n(t)$, with $n(t) =$
 231 n_{max} corresponding to all available release sites containing a docked vesicle.

232 Synaptic stimulation results in vesicle release and hence changes in the RRVP, as
 233 given by:

$$\frac{dn(t)}{dt} = \frac{n_{max} - n(t)}{\tau_r(t)} - \sum_j \delta(t - t_j).p(t).n(t)$$

234 APs arrive at times t_j , resulting in vesicle release and depletion of the RRVP. The
 235 RRVP is replenished with time constant, τ_r , from an effectively infinite reserve pool
 236 and may reach a maximum size n_{max} . During HFS τ_r is small due to fast, activity-
 237 dependent recovery (Hennig et al., 2008) and its initial value, τ_{r0} is obtained from
 238 fitting to the initial phase (0.5 s) of depression during stimulation. To model extra
 239 depression of the EPSC amplitude during HFS in zero glucose, τ_r is allowed to
 240 increase in value during the HFS (see below). During recovery, the replenishment
 241 rate at the end of the HFS, τ_{rH} increases rapidly, with time constant τ_d , to a slower
 242 background rate (larger time constant), τ_{rR} , according to:

$$\tau_r(t) = \tau_{rH} + (\tau_{rR} - \tau_{rH}) / (1 - e^{-t/\tau_d})$$

243 The experimental data shows that glucose depletion results in a greater EPSC
 244 depression during HFS followed by recovery to a lower maximum EPSC amplitude,
 245 while the rate of recovery is not significantly slower. Two factors are used to capture
 246 this behaviour in the model. Firstly, the increased depression during HFS is modelled
 247 by increasing τ_r during the HFS (thus slowing activity-dependent replenishment of
 248 the RRVP and so reducing n) according to a logistic function:

$$\tau_r(t) = \tau_{r0} / [A_n + (1 - A_n) / (1 + e^{(t-t_n)/k_n})]$$

249 where A_n is the steady-state fractional increase in τ_r reached following HFS (final τ_r
 250 denoted τ_{rH}), t_n is the half-time increase, and k_n determines the rate of the increase
 251 (larger k_n means slower increase). To model the recovery to a reduced EPSC
 252 amplitude, the maximum RRVP size, $n_{max}=1$ during HFS, is set to a lower value,
 253 $n_{max}=n_{rec}$, during the recovery phase, implying a reduction in the number of functional
 254 release sites.

255 Facilitation of release probability, $p(t)$, is modelled by increasing the release
 256 probability by the amount $k_f \cdot (1 - p(t))$ after each presynaptic AP. Release
 257 probability then decays with time constant τ_f to base release probability $c(t)$:

$$\frac{dp(t)}{dt} = \frac{c(t) - p(t)}{\tau_f} + \sum_j \delta(t - t_j) \cdot k_f \cdot (1 - p(t))$$

258 The variable $c(t)$ (initialised to P_0) accounts for a slow depression of p , underpinning
 259 the slow rundown in EPSC amplitude during long stimulations (Hennig et al., 2008).
 260 Each presynaptic AP reduces $c(t)$ by $k_i \cdot c(t)$ which then recovers to its resting value
 261 P_0 with a time constant τ_i :

$$\frac{dc(t)}{dt} = \frac{P_0 - c(t)}{\tau_i} - \sum_j \delta(t - t_j) \cdot k_i \cdot c(t)$$

Automated non-linear curve fitting was used to fit simulated normalised EPSC amplitudes to experimentally obtained EPSCs during HFS followed by a recovery period. Peak EPSC amplitudes were extracted from each experimental recording to give the data against which the model was optimised.

Since the electrophysiological recordings only contain one stimulation frequency, one parameter value was fixed to reduce the degrees of freedom in the fitting: in these recording conditions, the facilitation fraction, k_f , balances somewhat the value of the facilitation time constant, τ_f , so its value has been fixed to 0.03 and only τ_f is identified.

Parameter identification proceeded as follows:

1. Parameters τ_{r0} , p_0 , and τ_f were identified from the first 0.5 s of HFS (other slower model components were not present).
2. With the above parameter values fixed, the remaining parameters were identified from the remaining period of HFS (29.5 s) plus the recovery period.
3. On entering recovery, the maximum RRVP size, n_{max} is set to a new value n_{rec} which is identified from the final, recovered steady-state EPSC amplitude.

All the simulations and the parameter identification procedure were implemented in Python 2.7. The model error was calculated as the sum-of squares difference between the model and mean experimental EPSC amplitudes at all stimulation time points. Parameter identification to minimise this error was done with the *fmin* function

of the *scipy.optimize* Python package. The model differential equations were numerically integrated with the *odeint* function of the *scipy.integrate* Python package.

Results

Impaired presynaptic function following glucose deprivation

The aim was to manipulate energy supply selectively to the presynaptic terminal. The postsynaptic neuron was rendered independent of aCSF substrate availability by diffusion of ATP from the recording patch pipette (Figure 1A). Under control conditions slices were perfused with standard aCSF containing 10 mM glucose. The HFS paradigm (100 Hz, 30 s, i.e. 3000 evoked responses, Figure 1B) caused a profound depression of EPSC amplitude within 0.2 s in every case (Figure 1C, representative example) that continued at a slower rate throughout the continuing 30 s of stimulation (e.g. Figure 3A). The EPSC amplitude fully recovered within 20 s of the end of the HFS (Figure 1D, same recording as 1C). This HFS was repeated in four cells, at 5 min intervals, with no significant change in the magnitude of EPSC depression or recovery over 30 min. Each 5 min cycle of HFS is referred to as an 'HFS epoch'. This reproducible cycle of EPSC depression and recovery is plotted in Figure 1E (filled circles for the first and last EPSCs in the HFS and open circles for the recovery phase).

Depletion of energy substrate was achieved by switching to an aCSF containing zero glucose, Figure 1F shows the results of the HFS paradigm under this condition (Figure 1F). By the fourth epoch under the energy depleted condition, the EPSC amplitude was highly depressed (69.1 ± 7.9 % compared to 20.3 ± 12.6 % in 10 mM

glucose control). This observation is further analysed in Figure 2, where the raw and mean EPSC amplitudes for control (10 mM) and zero glucose conditions are plotted. After 20 min of zero glucose the EPSC amplitude had depressed by $89.2 \pm 3.3 \%$ (n=6) at the end of HFS, compared to $59.7 \pm 5.9 \%$ depression in controls with 10 mM glucose (n=4, Figure 2A, 2B for raw and normalised data, respectively; example EPSC traces in Figure 2D). The EPSC depression at the start of the HFS was similar in both conditions. However, during the last 8 s of HFS the magnitude of the depression significantly increased in the zero glucose condition compared with control (two-way RM-ANOVA, interaction $p < 0.001$, Bonferroni post hocs $p < 0.05$ for last 8 s of HFS; Figure 2B; at 25 minutes EPSCs had depressed by $54 \pm 6.0 \%$ in 10 mM glucose and $79.6 \pm 5.5 \%$ with 0 mM glucose; interaction $p < 0.001$, Bonferroni post hocs $p < 0.05$ for last 8 s of HFS, power = 88.4 %). The recovery of EPSC amplitude was best fit by a double exponential under control conditions (10 mM glucose, $\tau_{\text{fast}} 226 \pm 117$ ms (44% amplitude ratio); $\tau_{\text{slow}} 2.6 \pm 2.5$ s) but after 20 min of zero glucose the rapid phase of recovery was lost (Figure 2C), and recovery was best fit by a slow exponential ($\tau 4.3 \pm 0.6$ s). In control conditions the EPSC amplitude fully recovered ($94.8 \pm 8.4\%$ of first EPSC, t-test, $p = 0.58$), but in the absence of glucose the EPSC amplitude failed to fully recover by 20 s after the HFS ($61.4 \pm 14.9 \%$ of first EPSC, t-test, $p = 0.048$), and remained depressed after 4 min of rest without stimulation (i.e. between epochs).

The decreased EPSC amplitude could reflect a reduction in either release probability or in the size of the RRVP. Coefficient of variation (standard deviation/mean) and variance / mean were calculated to give an indication of which factors are dominant. EPSC amplitudes were measured to calculate their mean, variance and standard

deviation at early (3-4 s) and late (29-30 s) segments of the HFS train, since at these times the EPSC amplitudes were relatively stable. Mean EPSC amplitude is given by $n.p.q$, which has variance = $npq^2(1-p)$. Thus the variance/mean = $q(1-p)$ and CV = std dev/mean = $\sqrt{(1-p)/np}$. After 20 min without glucose the early coefficient of variation (0.10 ± 0.01 , $n=6$) was not significantly different from that measured in control (0.08 ± 0.01 , $n=4$; two-way repeated measures ANOVA, between groups $p=0.008$, Bonferroni post hoc $p>0.99$; Figure 2E left panel). However, the late coefficient of variation was significantly increased in the zero glucose condition (0.23 ± 0.03) compared to control (0.10 ± 0.01 , Bonferroni post hoc $p=0.01$). CV depends on both n and p (but not q), while var/mean depends on q and p . Since the var/mean was the same for all (two-way repeated measures ANOVA, between groups $p=0.99$; Figure 2E right panel), q and p can be assumed to both be stable across time points and conditions, hence the increase in CV late in the HFS with zero glucose, must be due to a decrease in n . This discounts a decrease in release probability as a major cause of the decrease in EPSC amplitude during HFS, and so the increase in coefficient of variation in zero glucose is likely caused by a decrease in the RRVP size.

HFS given after 25 min of continued perfusion of zero glucose resulted in EPSC failures in 3 out of 4 cells (Figure 2F, timing of failures are indicated by filled triangles). Throughout these experiments the postsynaptic neurons (that had maintained ATP from the patch pipette) had stable holding currents (data not shown).

ATP depletion reduced RRVP size and the number of functional release sites.

The above experimental data was used to fit a model of transmission at the calyx of Held from which presynaptic release parameters could be estimated. The model produced very good fits in both 10 mM ($n=4$) and zero glucose conditions to the normalised, averaged EPSC data ($n=5$, except for 25 min where $n=3$; Goodness of fit values all 0.99; Figure 3A-D). The early phase of HFS (0.5 s) was well fit by a combination of a facilitating release probability, p , and a depressing RRVP size, n , that recovered at a fast, activity dependent rate (time constant, τ_{r0} , on the order of 50 msec; Table 1; Figure 4A-D insets). The identified values for the initial release probability (P_0), facilitation (τ_f) and initial activity-dependent vesicle recovery rate (τ_{r0}) were consistent between control and zero glucose conditions and across all epochs (Table 1). Slow depression of release probability sees p settle at stable values after around 5 secs of HFS (Figure 4C,D), while the RRVP size, n , continues to decline due to a slowing of the activity-dependent replenishment rate (Figure 4A,B). The slowing of replenishment was greatly enhanced in the later epochs in zero glucose (Figure 4B). The time course of recovery was dominated by the slow recovery of the release probability, with residual activity-dependent replenishment allowing the RRVP size to recover quickly.

The model captured the enhanced EPSC depression during HFS as glucose concentration declined during the sequential epochs (Figure 3B-D) as an increase in the activity-dependent replenishment time constant, τ_r , resulting in a decrease in the RRVP size (Figure 4B). This reduction in RRVP size (n) was largely sufficient to account for the increase in coefficient of variation of EPSC amplitude measured in the experimental data. The increase in coefficient of variation during HFS at 20 min in zero glucose (Figure 2E left panel) was consistent with n decreasing by a factor of

5.3 (assuming release probability or quantal size do not change) and the model predicted a change of 4.5.

The impaired EPSC recovery following HFS was captured in the model by a sustained reduction in the maximum RRVP size (functional release sites) where recovery became increasingly incomplete over the 15, 20 or 25 min epochs (Figure 4B and Table 1).

Vesicular cycling was measured without dialysis of the presynaptic terminal, by imaging vesicles that were labelled using the styryl dye FM1-43FX, in slices perfused with 10 mM glucose and zero glucose aCSF (Figure 5A). Vesicles were labelled by applying FM1-43FX immediately before the 20 min HFS epoch, and the rate of release was subsequently measured by washing out the dye and imaging at 2 Hz during the HFS at 25 minutes. We observed a faster rate of release in 10 mM glucose compare to zero glucose (Figure 5B), consistent with the impaired synaptic transmission observed while monitoring EPSCs in zero glucose (Figure 2). A measure of synaptic vesicles labelled with FM1-43FX during the 20 min epoch, was made after α -Latrotoxin induced FM-destaining following the 25 min HFS to ensure exocytosis of all labelled vesicles. The ratio of FM-dye fluorescence after α -Latrotoxin over fluorescence after labelling (F_{Lat}/F_0) is significantly lower for synapses perfused with 10 mM glucose (n=14) compared with the ones perfused with zero glucose (n=12, t-test, $p<0.001$; Figure 5B), suggesting that a smaller number of vesicles underwent release and endocytosis at the 20 min epoch in zero glucose compared to 10 mM glucose.

Reducing presynaptic ATP levels impairs vesicle replenishment

We have assumed that the mechanism underlying impaired presynaptic function during glucose depletion was caused by reduced presynaptic ATP; to test this hypothesis, paired pre- and postsynaptic recordings were performed where the presynaptic ATP concentration was changed by dialysis from the pipette (while monitoring synaptic transmission). The experimental paradigm is shown in Figure 6A and example EPSCs in Figure 6B.

ATP hydrolysis was blocked in the terminal by diffusion of 2.2 mM ATP γ S (a non-hydrolysable analog of ATP) from the presynaptic patch pipette and this was compared to a control condition where the pipette contained 2.2 mM ATP. After 1-2 min of dialysis the depression of EPSC amplitude during HFS was similar with either ATP or ATP γ S in the presynaptic pipette (ATP γ S, 51.5 ± 8.2 %, $n=5$; compared to ATP, 53.0 ± 9.8 %, $n=7$; two-way RM-ANOVA, between groups $p=0.91$, interaction $p=0.16$; Figure 6C,D). However, even at this early time-point, the EPSC recovery was slowed by ATP γ S (ATP, $\tau 4.4 \pm 1.0$ s and ATP γ S, $\tau 12.2 \pm 14.4$ s) so that EPSC recovery was significantly impaired in the presence of ATP γ S compared to ATP (two-way RM-ANOVA, between group $p<0.01$). The EPSC amplitude fully recovered by 30 s after the end of the HFS with ATP in the patch pipette (85.5 ± 7.9 % of first EPSC, t-test, $p=0.12$), but remained significantly depressed with ATP γ S in the pipette (41.3 ± 8.4 % of first EPSC, t-test, $p=0.002$; Figure 6E). When HFS was repeated 5 min later, EPSC amplitude had not recovered; the raw EPSC amplitude at the start of the second HFS was only 0.72 ± 0.32 nA ($n=5$) with ATP γ S, compared to 4.9 ± 0.8 nA ($n=12$) with ATP (data not shown). This pharmacological block of ATP hydrolysis supports the interpretation that the compromised transmission with glucose depletion was due to lack of ATP.

424 To more closely mimic the presynaptic condition occurring with glucose depletion, a
425 less extreme protocol was required, so presynaptic paired recordings were repeated
426 and presynaptic ATP lowered from 2.2 to 0.1 mM (without adding ATPyS). The total
427 adenine nucleotide concentration in the presynaptic pipette was maintained constant
428 at 2.2 mM (Jolivet et al., 2015), so for the low (0.1 mM) ATP condition, 2.1 mM AMP
429 was added to the presynaptic pipette. Under these conditions HFS within 1-2 min of
430 breaking into the presynaptic terminal resulted in an EPSC depression with low ATP
431 in the pipette (69.0 ± 2.9 %, $n=8$) that was similar to that with high ATP (53.0 ± 9.8
432 %, $n=7$; two-way RM-ANOVA, between groups $p=0.12$, interaction $p=0.45$; power
433 35%, Figure 6F,G). The time course of EPSC amplitude recovery in the low ATP
434 condition was significantly altered (two-way RM-ANOVA, interaction $p<0.001$,
435 between groups $p=0.15$), but in both high and low ATP conditions EPSC amplitude
436 had recovered by 30 s after HFS (high ATP alone 85.5 ± 7.9 % of first EPSC, t-test,
437 $p=0.12$; low ATP 102.3 ± 4.3 % of first EPSC, t-test, $p=0.61$; Figure 6H). The
438 recovery curves were best fit with a single exponential (high ATP $\tau 4.4 \pm 1.0$ s, low
439 ATP $\tau 12.5 \pm 2.3$ s). HFS was repeated 6-7 min after breaking into the presynaptic
440 terminal once there had been more time for dialysis to occur. In the low ATP
441 condition the EPSC depression (85.7 ± 2.2 %, $n=12$) was significantly increased
442 compared to the high ATP condition (70.0 ± 2.8 %, $n=12$; two-way RM-ANOVA,
443 between groups $p<0.001$, interaction $p=0.17$; Figure 6B,I,J). There was a significant
444 difference between the high and low ATP groups in the magnitude of EPSC
445 amplitude during recovery (two-way RM-ANOVA, between groups $p=0.011$;
446 power=99 %, Figure 6B,K). The recovery curves were best fit with single
447 exponentials (high ATP $\tau 6.9 \pm 0.5$ s; low ATP $\tau 7.4 \pm 1.1$ s; Fig 6K). EPSC amplitude
448 failed to fully recover within 30 s after the HFS with low presynaptic ATP (69.2 ± 4.5

% of first EPSC, t-test, $p < 0.001$), and while the magnitude of the recovery was greater with high presynaptic ATP the EPSC amplitude failed to fully recover (83.5 ± 5.7 % of first EPSC, t-test, $p = 0.01$). These results indicate that high frequency transmission and subsequent EPSC recovery require presynaptic ATP, but also that dialysis of the presynaptic terminal alters vesicle recycling even when a high concentration of ATP is supplied.

These data therefore confirm that the changes observed in synaptic transmission on removal of glucose are a consequence of presynaptic ATP depletion from the terminal with subsequent impaired vesicle recycling. Having set up a means to investigate metabolic demand in a functional synapse, we asked to what extent other substrates substitute for glucose and tested the astrocyte-neuron lactate shuttle (ANLS) hypothesis.

At physiological glucose concentrations the lactate shuttle is required for maintenance of presynaptic function

We tested whether the lactate shuttle was an important energy source for presynaptic terminals at physiological glucose concentrations, by blocking lactate uptake with monocarboxylate transporter (MCT) inhibitors. For these experiments we returned to only patching the postsynaptic MNTB neuron and using electrical stimulation of the calyx axons to evoke HFS and recovery pulses at 5 min intervals. We used a combination of two MCT inhibitors: 200 μ M 4-CIN, a competitive MCT2 inhibitor (IC_{50} 24 μ M in *Xenopus* oocytes, Broer et al., 1999), and 1 μ M AR-C155858, a non-competitive MCT1/2 inhibitor that diffuses into cells and binds to the intracellular domain of the MCTs (K_i 2-10 nM in rat erythrocytes and *Xenopus* oocytes, Ovens et al., 2010). This combination of MCT inhibitors was found to be

effective at blocking transmission supported by lactate in the absence of glucose (Figure 7). Even in the presence of a high concentration of lactate (10 mM) the MCT inhibitors reduced the EPSC amplitude to 0.95 ± 0.51 nA (n=3) by 30 min, compared to an EPSC amplitude of 7.35 ± 1.27 nA (n=4) in 10 mM lactate alone.

In initial experiments, we found that application of MCT inhibitors for 30 mins in the presence of 10 mM glucose did not significantly increase the EPSC depression during HFS or reduce the fast component of EPSC recovery (data not shown). While 10 mM is a standard glucose concentration used for *in vitro* brain slice electrophysiology, a more realistic extracellular glucose concentration in the brain is in the range of 1-2 mM, while lactate levels are around 2-5 mM (Zilberter et al., 2010). We therefore investigated energy substrate use by the presynaptic terminal at more physiological concentrations by examining whether 1 mM glucose or 1 mM lactate could maintain presynaptic function and tested the extent to which lactate shuttled from glial cells contributed to presynaptic energy supply at physiological glucose concentrations.

After 30 minutes of perfusion with aCSF containing 1 mM glucose the EPSC depression during HFS (59.5 ± 3.0 %, n=10) was not significantly different to that with 10 mM glucose (50.9 ± 3.0 %, n=4, two-way RM-ANOVA, between group $p=0.007$, Dunnett's post hoc, $p=0.35$; power=53 %, Figure 8A,B,F). In the absence of glucose, 1 mM lactate can maintain synaptic function, with depression of 64.8 ± 7.9 % during HFS (n=4); this was not significantly different to that seen in the presence of 1 mM glucose (Dunnett's post hoc $p=0.71$; power=9 %, Figure 8A,B,F). The next question was to determine if the presynaptic terminal was using glucose directly or relying on the lactate shuttle. Perfusion of the MCT inhibitors in the presence of 1 mM glucose depressed EPSCs during HFS by 75.3 ± 3.5 % (n=6), which was

498 significantly greater than the depression seen with 1 mM glucose alone (59.5 ± 3.0
499 %, $n=10$, Dunnett's post hoc, $p=0.017$; power=93 %, Figure 8C,D,F). This suggests
500 that the presynaptic terminal is using glucose and that additional lactate (presumably
501 from glial cells) is important for maintaining normal transmission.

502 The recovery of the EPSC amplitude following HFS was not found to be significantly
503 different between the 1 mM glucose, 1 mM lactate or 1 mM glucose plus MCT
504 inhibitor groups (two-way RM-ANOVA, between groups $p=0.21$, interaction $p=0.36$;
505 Figure 8E). In all conditions the EPSC amplitude fully recovered within 20 s after the
506 end of HFS (1 mM glucose 94.3 ± 6.0 % of first EPSC, t-test, $p=0.37$; 1 mM lactate
507 97.2 ± 13.1 % of first EPSC, t-test, $p=0.85$; 1 mM glucose plus MCT inhibitors $94.2 \pm$
508 7.3 % of first EPSC, t-test, $p=0.46$). In all conditions the recovery was best fit by a
509 double exponential (1 mM glucose τ_{fast} 310 ± 47 ms, 31 %, τ_{slow} 5.8 ± 10.6 ; 1 mM
510 lactate τ_{fast} 277 ± 31 ms, 32 %, τ_{slow} 5.9 ± 0.3 s; 1 mM glucose with the MCT
511 inhibitors in the presence of 1 mM glucose τ_{fast} 193 ± 62 ms, 23 %, τ_{slow} 5.5 ± 0.6 s).

512 Recovery curves are generally fit to the mean EPSC amplitudes due to the large
513 degree of variability in individual experiments. However, this generalisation masks
514 elements of the physiological response, so for the mean recovery curves shown in
515 Figure 8E, we have re-plotted each individual recovery curve for each experiment in
516 Figures 9A-D. In the 1 mM glucose the recovery curves were best fit by a double
517 exponential in 8 out of 10 cases (Figure 9A, with 9B showing the fast component up
518 to 2.5 s), in two cases (indicated by black squares) only a single slow component
519 was observed. Similarly, in 1 mM glucose with the MCT inhibitors the best fit was a
520 double exponential in 5 out of 6 experiments (Figure 9C); again the one cell which
521 could not be fit by a double exponential is shown with black squares. In the 1 mM

lactate experiment, all four cases could be fit to a double exponential (Figure 9D). We show this data to justify exclusion of those small number of cases where the recovery curve is not fit by a double exponential, which then allows analysis of the fast and slow components of recovery. Analysing only the double exponential recovery curves, the percentage of fast recovery was significantly reduced in the presence of the MCT inhibitors ($25.3 \pm 3.3 \%$, $n=5$) compared to 1 mM glucose ($50.0 \pm 5.5 \%$, $n=8$, one-way ANOVA $p=0.02$, Dunnett's post hoc $p=0.01$; Figure 9E), consistent with a presynaptic contribution by metabolism of lactate under low glucose conditions. There was no significant difference in the percentage of fast recovery between 1 mM lactate ($33.8 \pm 8.4 \%$, $n=4$) compared to 1 mM glucose (Dunnett's post hoc $p=0.14$; Figure 9E). The value of the fast time constant was the same across all experimental conditions (1 mM glucose 440 ± 163 ms, 1 mM glucose plus MCT inhibitors 167 ± 43 ms, 1 mM lactate 342 ± 127 ms, one-way ANOVA $p=0.42$; Figure 9F). Similarly, the slow time constant was unchanged across all conditions (1 mM glucose 7.4 ± 1.6 s, 1 mM glucose plus MCT inhibitors 4.5 ± 2.0 s, 1 mM lactate 7.3 ± 1.9 s, one-way ANOVA $p=0.48$; Figure 9G). We conclude that the underlying recycling processes were unchanged across these conditions, and that loss of lactate as a presynaptic substrate (by blocking uptake) reduced ATP availability and that this was reflected in a reduced fast activity-dependent recovery.

Under low ATP conditions the Thr172 residue of AMP kinase is phosphorylated, so phospho-Thr172-AMPK is used as an indicator of metabolic stress (Hardie et al., 2012). We tested for evidence of metabolic stress using western blotting from slices that had been used for electrophysiology. In slices treated with 1 mM glucose (for 40 min) there was increased AMPK Thr172 phosphorylation compared to slices treated

with 10 mM glucose (Figure 8G) and the addition of the MCT inhibitors in the presence of 1 mM glucose did not further increase AMPK phosphorylation.

To determine whether the lactate supporting presynaptic function was generated from glucose or the result of glycogen breakdown within glial cells, we applied the glycogenolysis inhibitor, 1,4-dideoxy-1,4-imino-d-arabinitol (DAB, 500 μ M), in the presence of 1 mM glucose. We found no effect of DAB on the magnitude of EPSC depression during HFS (43.5 ± 5.3 %, $n=4$) when compared to glucose alone (49.3 ± 3.3 % $n=4$; two-way RM-ANOVA, between groups $p=0.38$, interaction $p=0.88$, power=15 %, Figure 10A,B,D). Furthermore, there was no significant effect on the EPSC amplitude during the recovery period (two-way RM-ANOVA, between groups $p=0.86$, interaction $p=0.20$), and the recovery curve in the presence of 1 mM glucose plus DAB was fit by a double exponential (τ_{fast} 157 ± 25 ms, 59 %, τ_{slow} 7.8 ± 2.6 s, Figure 10C). We conclude that there is no detectable contribution from glycogenolysis when glucose is available in the aCSF.

Lactate produced from glycogenolysis in glial cells helps support presynaptic function in extreme glucose deprivation.

Lactate contributes to maintaining synaptic transmission in low glucose, but what happens during more severe energy deprivation, such as when glucose was being completely depleted? Synaptic transmission was maintained for 15 min during perfusion of an aCSF containing zero glucose and zero lactate. The EPSC depression was 45.2 ± 4.6 % during HFS ($n=6$; Figure 11A,B), but the addition of MCT inhibitors (in the same zero glucose/lactate aCSF) significantly increased the magnitude of the EPSC depression to 65.4 ± 4.0 % ($n=6$, two-way RM-ANOVA, between groups $p=0.01$, Bonferroni post hoc, $p=0.01$). Perfusion of the

glycogenolysis inhibitor (500 μ M DAB, in zero glucose/lactate aCSF) increased the magnitude of EPSC depression to 62.3 ± 4.1 % ($n=7$, Bonferroni post hoc, $p=0.03$; power=79 %, Figure 11A,B,D). There was no significant difference in the EPSC depression between the MCT inhibitor and DAB groups (Bonferroni post hoc, $p>0.99$). The EPSC recovery phase in zero glucose/lactate aCSF maintained both fast 142 ± 34 ms (30 %) and slow 2.7 ± 0.3 s components; and was not significantly different on addition of MCT inhibitors (τ_{fast} 201 ± 88 ms, 15 %; τ_{slow} 9.4 ± 1.1 s; Figure 11C) or DAB (τ_{fast} 351 ± 85 ms, 31 %; τ_{slow} 7.4 ± 0.8 s; two-way RM-ANOVA, between group $p=0.084$, interaction $p=0.64$). The HFS epochs were continued every 5 mins (beyond this 15 mins time point) until EPSC failures started to occur. In the DAB condition, but not with the MCT inhibitors, the first EPSC failure occurred earlier than with zero glucose alone (one-way ANOVA, $p=0.033$; Bonferroni post hocs, DAB $p=0.03$, MCT inhibitors $p=0.50$; Figure 11E). We conclude that during glucose deprivation lactate can help to maintain presynaptic function in the short-term, with the lactate being generated by the breakdown of stored glycogen.

Discussion

We have employed the calyx of Held/MNTB synapse to investigate how energy substrate availability and presynaptic ATP influence synaptic transmission. Synaptic transmission declines and eventually fails following glucose depletion. Dialysis of the presynaptic terminal with low ATP confirmed that the impaired transmission following glucose removal is caused by presynaptic ATP depletion. Model-based analysis of synaptic transmission indicated that glucose depletion slowed activity-dependent vesicle replenishment and reduced the number of functional release sites, resulting in a smaller resting RRVP size. When extracellular glucose is within the physiological

range (1 mM) the presynaptic terminal uses glucose and lactate. Glycogenolysis also contributes to the maintenance of synaptic transmission during glucose deprivation (Figure 12).

Presynaptic ATP depletion impairs presynaptic function

At the calyx of Held/MNTB synapse HFS generates a well characterised short-term synaptic depression, which is one way of reducing metabolic cost during prolonged transmission (Billups et al., 2005; von Gersdorff and Borst, 2002). Sustained HFS in the presence of 10 mM glucose caused an initial rapid depression in the EPSC amplitude followed by a period of relatively stable low amplitude EPSC transmission, which subsequently recovered to the initial EPSC amplitude. Twenty minutes after the removal of glucose, EPSC depression increased towards the end of the HFS train and recovery was impaired. Energy deprivation would eventually influence the postsynaptic resting membrane potential and conductance (Akasu et al., 1996; Calabresi et al., 1997), but in our experiments ATP was provided in the postsynaptic patch pipette, thereby eliminating postsynaptic effects while permitting depletion of the presynaptic terminal. Repeating HFS epochs over a period of 25 min without glucose caused a progressive decline in EPSC amplitude and failure of transmission.

Dialysis of ATPyS into the presynaptic terminal rapidly blocked all ATP usage. A more subtle control of presynaptic ATP was achieved by dialysis of the terminal with low ATP, this condition increased EPSC depression during HFS and impaired the subsequent recovery, similar to glucose deprivation. These results confirm that the effects of glucose deprivation were caused by presynaptic energy depletion and reduced glutamate release. This is consistent with glucose deprivation in other brain

regions where transmission is impaired by a reduction in transmitter release (Akasu et al., 1996; Calabresi et al., 1997; Izumi et al., 1997).

Energy deprivation reduces the number of functional release sites and rate of vesicle replenishment.

Analysis of the data and fit to the computational model suggests the reduction in synaptic transmission with ATP depletion is due to slowed activity-dependent replenishment of the RRVP during HFS and a decreased number of functional release sites, resulting in a reduced resting RRVP size following recovery (Figure 9). Reductions in vesicle release probability cannot account for EPSC amplitude changes since there was no change in the variance/mean ratio of EPSC amplitudes during the HFS. The initial release probability (P_o) early in the HFS was unchanged in the absence of glucose, consistent with there being sufficient time (4 minutes) and ATP availability to recover the release probability between HFS epochs. This contrasts with a previous study where glucose deprivation decreased the release probability in corticostriatal synapses (Calabresi et al., 1997).

The increased activity-dependent RRVP replenishment time constant, τ_r , is the major factor contributing to the increased EPSC depression during HFS in zero glucose. This is consistent with the loss of the fast activity-dependent component from the EPSC recovery curve after 20 min of zero glucose (Figure 2D), which corresponds with the slow release pool previously observed at the calyx and blocked by ATPyS (Neher, 2017; Sakaba and Neher, 2003). Furthermore, when the presynaptic terminal was dialysed with low ATP the first change was a slowing of recovery (Figure 6H), and block of presynaptic lactate uptake by MCT inhibitors reduced the

contribution by the fast recovery phase (Figure 8E, Figure 9), suggesting that activity-dependent vesicle replenishment is particularly sensitive to reduced presynaptic ATP.

The model identified a reduced size of the maximal RRVP as underlying the failure of the EPSC to fully recover between HFS trains with glucose deprivation. This is interpreted as an increase in the number of release sites lacking primed vesicles, which could arise by the slowing of multiple ATP-dependent processes, including vesicle priming and recycling. When glucose was removed, the imaging results suggest that endocytosis is particularly susceptible to energy depletion, while exocytosis is less so; this fits with previous findings that endocytosis is a particularly energy demanding process (Rangaraju et al., 2014; Pathak et al., 2015).

The action potential waveform is also capable of influencing transmitter release.

The relationship between presynaptic action potential waveform, calcium influx and transmitter release at the calyx of Held is well characterized and detailed (Borst & Sakmann, 1998; Kochubey et al., 2009; Yang & Wang, 2006; for reviews see von Gersdorff & Borst 2002; Schneggenburger & Forsythe, 2006). Changes in presynaptic AP waveform have been observed following blockade of potassium currents (Wang & Kaczmarek, 1998) in studies of activity-dependent vesicle recycling, and with activity-dependent modulation of presynaptic potassium currents at mossy fibres (Geiger & Jonas, 2000). Recent observations during resting conditions and low frequency stimulation (Lujan et al., 2016) support the idea that

pharmacological block of glycolysis affects transmitter release by depolarization (implying rundown of ionic gradients) and slowing of the presynaptic AP waveform. In the research reported in this paper, we have explored synaptic transmission under quasi-physiological conditions (*in vitro*) and induced a metabolic stress by exchanging extracellular metabolic substrates and induction of high frequency stimulation (with 3000 action potentials). Additionally, for the presynaptic recordings reported here, the 'action potential' was a voltage-clamp command and intracellular ionic concentrations were maintained by dialysis of the terminal from the patch pipette, so the changes in transmitter release observed with reduced ATP concentrations were not due to changes in AP waveform. This shows that mechanisms other than changes in AP waveform must also contribute, and we demonstrated that changes in neurotransmitter release parameters are observed on ATP depletion during high frequency stimulation.

Presynaptic terminals can utilise both glucose and lactate.

The ANLS hypothesis has stimulated considerable debate (Dienel, 2012; Pellerin and Magistretti, 2012). It postulates that during neuronal activity, when energy demand is high, glucose is preferentially metabolised by glial cells to lactate and this lactate is shuttled to neurons to meet neuronal metabolic demands (Pellerin and Magistretti, 1994). Many ANLS studies have been conducted in tissue culture, but the MNTB brain slice preparation has the advantage of maintaining association between the presynaptic calyx, its target neuron and glial cell (Uwechue et al., 2012). Izumi *et al.* (1997) found that lactate can fully support synaptic transmission, while others found 20 mM lactate could only partially substitute for glucose (Nagase et al.,

2014). We found that 1 mM lactate, which is within physiological ranges (Zilberter et al., 2010) can be metabolised by the terminal to sustain presynaptic function. Oxidative phosphorylation is the major energy source in the brain (Hall et al., 2012; Harris et al., 2012) with glucose metabolism rising with brain activity to drive local ATP synthesis (Rangaraju et al., 2014). Recent studies have suggested that glycolysis is very significant in nerve terminal metabolism (Ashrafi & Ryan, 2017; Lujan et al., 2016) and that neuronal activity increases Glut4 glucose transporters in presynaptic membranes (Ashrafi et al., 2017) via AMPK signalling, thereby raising intracellular pyruvate as a substrate for Krebs cycle.

The results demonstrate that when glucose is around physiological levels (1 mM) presynaptic terminals can utilise both glucose and lactate and that metabolic compromise during neuronal activity can limit the efficacy of synaptic transmission. Phosphorylation of AMPK-Thr172 did not increase when lactate uptake was blocked, suggesting that there was no further metabolic stress in the absence of lactate, but any further change may have been occluded through AMPK activation on reducing glucose from 10 to 1 mM. The ability to use both glucose and shuttled lactate will confer a physiological advantage where metabolic demands are high. In hippocampal slices the ANLS did contribute to maintaining synaptic transmission in slices exposed to low (2 mM), but not higher glucose concentrations (Izumi et al., 1997). Another study suggested that the ANLS is required for fully functional synaptic transmission (Nagase et al., 2014), however, 1 mM of the MCT inhibitor 4-CIN used in that study would be sufficient to also disrupt mitochondrial pyruvate uptake (McKenna et al., 2001) compromising Krebs cycle ATP production.

Glycogen is implicated as an energy source under physiological conditions (Suzuki et al., 2011; Brown et al., 2003). We found no evidence for glycogenolysis when neurons were supplied with 1 mM glucose, but during severe glucose deprivation MCT inhibitors and glycogenolysis inhibitors independently reduced synaptic transmission to a similar extent. In the brain, glycogen and glycogen phosphorylase (the enzyme required for glycogenolysis) are only found in glial cells (Cataldo and Broadwell, 1986; Pfeiffer et al., 1992). Our result under extreme glucose deprivation is consistent with lactate being produced by glial cells from the hydrolysis of glycogen stores to maintain synaptic transmission. Increases in the AMP:ATP ratio activate glycogen phosphorylase (Obel et al., 2012), consistent with glycogen acting as a short-term energy reserve to maintain neuronal transmission during glucose deprivation (Brown et al., 2003; Shetty et al., 2012). Alternatively, glial generation of lactate from glycogen could preserve extracellular glucose for neurons rather than generate lactate for neuronal use (DiNuzzo et al., 2010).

We demonstrate that excitatory synaptic terminals use glucose and lactate generated during glucose deprivation, consistent with lactate shuttling under conditions of metabolic stress. The experimental paradigms developed here to investigate presynaptic metabolic substrates in a physiological system show clear changes in synaptic transmission when energy supply is compromised or while sustaining high transmission rates. When energy resources become scarce modulation of presynaptic function may reduce metabolic demand, but will also compromise information transmission; the interplay between these signalling and metabolic pathways will provide insights to improve cognition following brain injury, for example in stroke, hypoglycaemia and ageing.

References

- Akasu T, Tsurusaki M & Shoji S (1996). Depletion of glucose causes presynaptic inhibition of neuronal transmission in the rat dorsolateral septal nucleus. *Synapse* **24**, 125-134.
- Ashrafi G, Wu Z, Farrell RJ & Ryan TA (2017). GLUT4 mobilization supports energetic demands of active synapses. *Neuron* **93**, 1-10.
- Ashrafi G & Ryan TA (2017). Glucose metabolism in nerve terminals. *Cur Opin Neurobiol* **45**, 156–161.
- Attwell D & Laughlin SB (2001). An energy budget for signaling in the grey matter of the brain. *J Cereb Blood Flow Metab* **21**, 1133-1145.
- Billups B, Graham BP, Wong AY & Forsythe ID (2005). Unmasking group III metabotropic glutamate autoreceptor function at excitatory synapses in the rat CNS. *J Physiol* **565**, 885-896.
- Borst JG & Sakmann B (1998). Calcium current during a single action potential in a large presynaptic terminal of the rat brainstem. *J Physiol* **506**, 143–157.
- Bröer S, Bröer A, Schneider HP, Stegen C, Halestrap AP & Deitmer JW (1999) Characterization of the high-affinity monocarboxylate transporter MCT2 in *Xenopus laevis* oocytes. *Biochemical Journal* **341**, 529-35.
- Brown AM, Tekkok SB, & Ransom BR (2003). Glycogen regulation and functional role in mouse white matter. *J Physiol* **549**, 501-512.

758 Calabresi P, Centonze D, Pisani A & Bernardi G (1997). Endogenous adenosine
 759 mediates the presynaptic inhibition induced by aglycemia at corticostriatal synapses.
 760 *J Neurosci* **17**, 4509-4516.

761 Cataldo AM & Broadwell RD (1986). Cytochemical identification of cerebral glycogen
 762 and glucose-6-phosphatase activity under normal and experimental conditions: I.
 763 Neurons and glia. *J Electron Microscopy Tech* **3**, 413-437.

764 Dienel GA (2012). Brain lactate metabolism: the discoveries and the controversies. *J*
 765 *Cereb Blood Flow Metab* **32**, 1107-1138.

766 DiNuzzo M, Mangia S, Maraviglia B & Giove F (2010). Glycogenolysis in astrocytes
 767 supports blood-borne glucose channeling not glycogen-derived lactate shuttling to
 768 neurons: evidence from mathematical modeling. *J Cereb Blood Flow Metab* **30**,
 769 1895-1904.

770 Duarte JM (2015). Metabolic Alterations Associated to Brain Dysfunction in Diabetes.
 771 *Aging Dis* **6**, 304-321.

772 Edelstein AD, Tsuchida MA, Amodaj N, Pinkard H, Vale RD, & Stuurman N (2014).
 773 Advanced methods of microscope control using µManager software. *J Biol Meth* **1**,
 774 1-10.

775 Feinkohl I, Aung PP, Keller M, Robertson CM, Morling JR, McLachlan S, Deary IJ,
 776 Frier BM, Strachan MW & Price JF (2014). Severe hypoglycemia and cognitive
 777 decline in older people with type 2 diabetes: the Edinburgh type 2 diabetes study.
 778 *Diabetes Care* **37**, 507-515.

779 Geiger JR & Jonas P (2000). Dynamic control of presynaptic Ca²⁺ inflow by fast-
 780 inactivating K⁺ channels in hippocampal mossy fiber boutons. *Neuron* **28**, 927–939.

781 Harata NC, Choi S, Pyle JL, Aravanis AM & Tsien RW (2006) Frequency-dependent
 782 kinetics and prevalence of kiss-and-run and reuse at Hippocampal synapses studied
 783 with novel quenching methods. *Neuron* **49**, 243-256.

784 Hardie DG, Ross FA & Hawley SA (2012). AMPK: a nutrient and energy sensor that
 785 maintains energy homeostasis. *Nat Rev Mol Cell Biol* **13**, 251-262.

786 Hall CN, Klein-Flügge MC, Howarth C & Attwell D (2012). Oxidative phosphorylation,
 787 not glycolysis, powers presynaptic and postsynaptic mechanisms underlying brain
 788 information processing. *J Neurosci* **32**, 8940–8951.

789 Harris JJ, Jolivet R & Attwell D (2012). Synaptic energy use and supply. *Neuron* **75**,
 790 762-777.

791 Hennig MH, Postlethwaite M, Forsythe ID & Graham BP (2008). Interactions
 792 between multiple sources of short-term plasticity during evoked and spontaneous
 793 activity at the rat calyx of Held. *J Physiol* **586**, 3129-3146.

794 Izumi Y, Benz AM, Katsuki H & Zorumski CF (1997). Endogenous monocarboxylates
 795 sustain hippocampal synaptic function and morphological integrity during energy
 796 deprivation. *J Neurosci* **17**, 9448-9457.

797 Jolivet R, Coggan JS, Allaman I & Magistretti PJ (2015). Multi-timescale modeling of
 798 activity-dependent metabolic coupling in the neuron-glia-vasculature ensemble.
 799 *PLoS Comp Biol* **11**, e1004036.

800 Kochubey O, Han Y & Schneggenburger R (2009). Developmental regulation of the
 801 intracellular Ca^{2+} sensitivity of vesicle fusion and Ca^{2+} -secretion coupling at the rat
 802 calyx of Held. *J Physiol* **587**, 3009–3023.

803 Kopp-Scheinflug C, Steinert JR & Forsythe ID (2011). Modulation and control of
804 synaptic transmission across the MNTB. *Hearing Res* **279**, 22-31.

805 Lujan B, Kushmerick C, Banerjee TD, Dagda RK & Renden R (2016). Glycolysis
806 selectively shapes the presynaptic action potential waveform. *J Neurophysiol* **116**,
807 2523-2540.

808 McKenna MC, Hopkins IB & Carey A (2001). Alpha-cyano-4-hydroxycinnamate
809 decreases both glucose and lactate metabolism in neurons and astrocytes:
810 implications for lactate as an energy substrate for neurons. *J Neurosci Res* **66**, 747-
811 754.

812 Meyer AC, Neher E & Schneggenburger R (2001). Estimation of quantal size and
813 number of functional active zones at the calyx of Held synapse by nonstationary
814 EPSC variance analysis. *J Neurosci* **21**, 7889-7900.

815 Nagase M, Takahashi Y, Watabe AM, Kubo Y & Kato F (2014). On-site energy
816 supply at synapses through monocarboxylate transporters maintains excitatory
817 synaptic transmission. *J Neurosci* **34**, 2605-2617.

818 Neher E. (2017). Some subtle lessons from the calyx of Held synapse. *Biophys J*
819 **112**, 215-223.

820 Obel LF, Muller MS, Walls AB, Sickmann HM, Bak LK, Waagepetersen HS &
821 Schousboe A (2012). Brain glycogen-new perspectives on its metabolic function and
822 regulation at the subcellular level. *Front Neuroenergetics* **4**, 3.

823 Ovens MJ, Davies AJ, Wilson MC, Murray CM & Halestrap AP (2010). AR-
824 C155858 is a potent inhibitor of monocarboxylate transporters MCT1 and MCT2 that

825 binds to an intracellular site involving transmembrane helices 7-10. *Biochemical*
826 *Journal* **15**, 523-30.

827 Pathak D, Shields LY, Mendelsohn BA, Haddad D, Lin W, Gerencser AA, Kim
828 H, Brand MD, Edwards RH & Nakamura K (2015). The role of mitochondrially
829 derived ATP in synaptic vesicle recycling. *JBC* **290**, 22325-36.

830 Pellerin L & Magistretti PJ (1994). Glutamate uptake into astrocytes stimulates
831 aerobic glycolysis: a mechanism coupling neuronal activity to glucose utilization.
832 *PNAS, USA* **91**, 10625-10629.

833 Pellerin L & Magistretti PJ (2012). Sweet sixteen for ANLS. *J Cereb Blood Flow*
834 *Metab* **32**, 1152-1166.

835 Perkins GA, Tjong J, Brown JM, Poquiz PH, Scott RT, Kolson DR, Ellisman MH &
836 Spirou GA (2010). The micro-architecture of mitochondria at active zones: electron
837 tomography reveals novel anchoring scaffolds and cristae structured for high-rate
838 metabolism. *J Neurosci* **30**, 1015-1026.

839 Pfeiffer B, Meyermann R & Hamprecht B (1992). Immunohistochemical co-
840 localization of glycogen phosphorylase with the astroglial markers glial fibrillary
841 acidic protein and S-100 protein in rat brain sections. *Histochemistry* **97**, 405-412.

842 Rangaraju V, Calloway N & Ryan TA (2014). Activity-driven local ATP synthesis is
843 required for synaptic function. *Cell* **156**, 825-835.

844 Sakaba T & Neher E (2003). Involvement of actin polymerization in vesicle
845 recruitment at the calyx of Held synapse. *J Neurosci* **23**, 837-846.

846 Satzler K, Sohl LF, Bollmann JH, Borst JG, Frotscher M, Sakmann B & Lubke JH
847 (2002). Three-dimensional reconstruction of a calyx of Held and its postsynaptic

848 principal neuron in the medial nucleus of the trapezoid body. *J Neurosci* **22**, 10567-
849 10579.

850 Schneggenburger R & Forsythe ID (2006). The calyx of Held. *Cell Tissue Res* **326**,
851 311–337.

852 Schindelin J, Arganda-Carreras I, Frise E, Kaynig V, Longair M, Pietzsch
853 T, Preibisch S, Rueden C, Saalfeld S, Schmid B, Tinevez J.Y. White, DJ, Hartenstein
854 V., Eliceiri K, Tomancak P & Cardona A (2012) Fiji: an open-source platform for
855 biological-image analysis. *Nature Methods* **9**, 676-682.

856 Shetty PK, Sadgrove MP, Galeffi F & Turner DA (2012). Pyruvate incubation
857 enhances glycogen stores and sustains neuronal function during subsequent
858 glucose deprivation. *Neurobiol Dis* **45**, 177-187.

859 Simpson IA, Carruthers A & Vannucci SJ (2007). Supply and demand in cerebral
860 energy metabolism: the role of nutrient transporters. *J Cereb Blood Flow Metab* **27**,
861 1766-1791.

862 Sokoloff L, Reivich M, Kennedy C, Des Rosiers MH, Patlak CS, Pettigrew, KD,
863 Sakurada, O & Shinohara M (1977). The [¹⁴C]deoxyglucose method for the
864 measurement of local cerebral glucose utilization: theory, procedure, and normal
865 values in the conscious and anesthetized albino rat. *J Neurochem* **28**, 897-916.

866 Steinert JR, Postlethwaite M, Jordan MD, Chernova T, Robinson SW & Forsythe ID
867 (2010). NMDAR-mediated EPSCs are maintained and accelerate in time course
868 during maturation of mouse and rat auditory brainstem in vitro. *J Physiol* **588**, 447–
869 463.

870 Suzuki A, Stern SA, Bozdagi O, Huntley GW, Walker RH, Magistretti PJ & Alberini
871 CM (2011). Astrocyte-neuron lactate transport is required for long-term memory
872 formation. *Cell* **144**, 810-823.

873 Uwechue NM, Marx MC, Chevy Q & Billups B (2012). Activation of glutamate
874 transport evokes rapid glutamine release from perisynaptic astrocytes. *J Physiol* **590**,
875 2317-2331.

876 von Gersdorff H & Borst JG (2002). Short-term plasticity at the calyx of Held. *Nat*
877 *Rev Neurosci* **3**, 53-64.

878 Wang LY & Kaczmarek LK (1998). High-frequency firing helps replenish the readily
879 releasable pool of synaptic vesicles. *Nature* **394**, 384–388.

880 Wong AY, Graham BP, Billups B & Forsythe ID (2003). Distinguishing between
881 presynaptic and postsynaptic mechanisms of short-term depression during action
882 potential trains. *J Neurosci* **23**, 4868-4877.

883 Yang Y-M & Wang L-Y (2006). Amplitude and kinetics of action potential-evoked
884 Ca^{2+} current and its efficacy in triggering transmitter release at the developing calyx
885 of Held synapse. *J Neurosci* **26**, 5698–5708.

886 Zilberter Y, Zilberter T & Bregestovski P (2010). Neuronal activity in vitro and the *in*
887 *vivo* reality: the role of energy homeostasis. *TiPS* **31**, 394-401.

888

889

890

891

Figure/Table legends

Figure 1. The paradigm to investigate presynaptic metabolic influence on transmission at the calyx of Held synapse, *in vitro*.

(A) The recording configuration showing bipolar stimulation of the presynaptic axon and patch recording of EPSCs from the postsynaptic MNTB neuron under whole-cell voltage clamp. Metabolism in the postsynaptic MNTB neuron is maintained by ATP through dialysis from the patch pipette.

(B) One epoch of high frequency stimulation (HFS, 50 s duration) consisted of a 30 s 100 Hz train, and a 20 s recovery phase of 6 stimuli (lower trace), the 3000 EPSCs from this train are plotted (middle trace) and single EPSC traces for the first and last EPSCs of the HFS train are plotted (top). The 6 Recovery EPSCs are plotted superimposed (with latencies after the HFS indicated in seconds) illustrating the recovery period.

(C) The percent EPSC amplitude is plotted normalised to the first EPSC, for one 30 s HFS (in standard recording conditions, 10 mM glucose). The initial rapid depression of EPSC amplitude over the first 0.1 s is shown in the inset; and EPSC amplitude is maintained at around 40% of the initial amplitude for the remainder of the HFS.

(D) The recovery of EPSC amplitude over 20 s following the end of HFS (in standard recording conditions, 10 mM glucose) shows full recovery within 20 s.

(E & F) HFS epochs were repeated at 5 minute intervals while recording over a period of 25 minutes. The mean EPSC amplitude (nA, not normalised) is plotted for the first and last EPSC of each HFS (filled circles) and for each of the recovery EPSCs (open circles) for control conditions with 10 mM extracellular glucose (E, n=4) and for zero extracellular glucose (F, n=5, except at 10 min where n=4). (E) For

the 10 mM glucose condition, EPSC amplitude recovers after each HFS and continues to do for each subsequent HFS epochs. (F) In zero glucose good recovery is observed after the first HFS epoch, but is increasingly compromised and incomplete during subsequent epochs, giving a progressive reduction in EPSC over time; so that there is little recovery from the third HFS epoch by 25 min (far right, black arrows) in the absence of glucose. Pooled data, mean \pm SEM.

Figure 2. Removal of glucose increases EPSC depression during HFS and impairs subsequent EPSC recovery.

(A) Raw EPSC amplitudes during a HFS epoch after 20 minutes in either 10 mM glucose (grey, n=4) or zero glucose (black, n=6). Left inset shows EPSC amplitudes for the first 0.1 s of the HFS. Right inset shows the potential sources of presynaptic metabolic substrate.

(B) The same data as A, under both conditions normalised to the amplitude of the first EPSC and pooled (mean \pm SEM). Left inset shows mean normalised EPSC amplitude for the first 0.1 s of the HFS. Right inset shows example traces of the first 5 EPSCs.

(C) Mean % normalised EPSC recovery curve at 20 minutes for 10 mM glucose and the impaired recovery after 20 min of zero glucose.

(D) Traces from one example after 20 min of zero glucose (top trace) showing 50 s HFS epoch and recovery. Single EPSC traces for the first and last EPSCs in the same HFS train are shown with 6 superimposed EPSCs (at the indicated latencies after the HFS) illustrating the recovery period.

(E) After 20 min of perfusion with either 10 mM glucose or zero glucose the coefficient of variation of the EPSCs was not different early in the HFS (3-4 s), but

was increased at the end of HFS (29-30 s) in the zero glucose condition (left panel). No change was seen in variance/mean between the two conditions at either time point (right panel).

(F) After 25 min of zero glucose EPSC failures were observed in three out of the 4 synaptic pairs studied; while no failures were observed in 10 mM glucose. In zero glucose the raw EPSC amplitude was further reduced and the magnitude of depression increased during HFS. The first failure for each recording is indicated by the black triangle. Left inset shows EPSC amplitudes for the first 0.1 s of the HFS. Right inset shows example traces of the first 5 EPSCs in each HFS train.

Figure 3. Model data fits well to experimental recordings.

The fit of the model (10 mM glucose in blue; zero glucose in red) to transmission in the two experimental conditions is overlaid with the mean experimental data (zero glucose in black, $n=5$ (25 min $n=3$); 10 mM glucose in grey, $n=4$) for four HFS epochs recorded at (A) 10 min, (B) 15 min, (C) 20 min and (D) 25 min. The model was fit to the 30 s HFS and the 20 s recovery period. Insets show the model fit and mean experimental data over the first 0.5 s of the experimental recordings. With increasing time, the zero glucose condition showed increased depression during the HFS (0-30 s) and slowed recovery in amplitude during the recovery phase (30-50 s).

Figure 4. The model parameters during glucose washout are consistent with a reduced number of functional release sites.

Plots of n (number of functional release sites) and p (release probability) model parameters for control 10 mM glucose (A & C) and zero glucose conditions (B & D) over the 10-25 mins of HFS epochs (10 – black, 15 - grey, 20 - blue, 25 - red).

(A) Decrease in the number of functional release sites (n) during HFS in aCSF containing 10 mM glucose. The relative change in the model parameter n (Initially $n=1$) from the beginning of each HFS epoch against time (s) is shown. The value of n is unchanged across all epochs. (B) Relative change in n during washout of glucose (zero glucose aCSF). In zero glucose, n decreases further and recovers more slowly during subsequent HFS trains (15, 20 and 25 min). (C) Although variable between epochs, no consistent change in release probability (p) was observed during each sequential HFS epoch (10, 15, 20, 25 min) in 10 mM glucose or (D) zero glucose.

Figure 5. Suppressed uptake of FM1-43 fluorescence following HFS during washout of glucose.

(A) Representative images of calyx of Held synapses labelled with FM1-43FX; labelling of vesicles in the presynaptic calyx is shown in green surrounding a central unstained (black) MNTB neuron. Left column shows 10 mM glucose the right column shows zero glucose before HFS (top), after HFS (middle) and after 2 min application of α -Latrotoxin (bottom). Scale bar 10 μ m.

(B) Summary graph of FM1-43FX fluorescence intensity plotted over time during the 25 min HFS (black bar) for calyces from slices perfused with 10 mM glucose (grey, $n=14$) and zero glucose (black, $n=12$). Inset: ratios of fluorescence intensity after Lat application over initial FM-dye fluorescence for calyces perfused in 10 mM glucose (grey, $n=14$) and zero glucose (black, $n=12$) show reduced vesicle recycling in the zero glucose condition.

Figure 6. Presynaptic dialysis with ATP γ S or low ATP enhances synaptic depression during HFS and impairs the subsequent EPSC recovery.

(A) Schematic of paired presynaptic and postsynaptic recording configuration (upper left) with the three ATP conditions for the presynaptic dialysis. ATP was always present in postsynaptic recordings. A voltage ramp (upper right) was applied to the presynaptic terminal to mimic an action potential and trigger transmitter release; the voltage ramp was applied to generate the HFS EPSC trains (100Hz, 2 sec) and the pulses to follow recovery (lower panel).

(B) Example EPSC traces recorded after 6-7 min presynaptic dialysis with high (2.2 mM) ATP (grey) or low (0.1 mM) ATP (red); the upper traces show full stimulation and recovery sweeps and the lower traces show the first and last EPSCs in the train (before recovery).

Data are presented to aid comparison as mean \pm SEM in a 3x3 matrix of plots. The columns: (C,F,I) Left - shows the mean raw EPSC amplitudes during the train; (D,G,J) Middle – shows the same data normalised to the amplitude of the first EPSC (100%); (E,H,K) Right – Normalised EPSC as % recovery curves.

The rows show the three experimental conditions:

(C,D,E) Top - ATP γ S (blue) versus ATP (grey) within 2 minutes of going 'whole-terminal'. This shows that dialysis with either ATP γ S or ATP for 1-2 minutes gave similar EPSC depression during the HFS, but the EPSC never recovered in the presence of ATP γ S.

(F,G,H) Middle – Low ATP (red) vs high ATP (grey) at 1-2 minutes of going 'whole-terminal'. Both ATP conditions gave a similar EPSC depression during the HFS; but recovery was slowed in the low ATP condition.

(I,J,K) Bottom – Low ATP vs high ATP after 6-7 minutes of dialysis. Longer dialysis with low ATP showed significant enhanced EPSC depression during the HFS and incomplete recovery afterwards.

Figure 7. Combined application of two MCT inhibitors generated an effective block of lactate uptake into the presynaptic terminal.

Slices were perfused with 10 mM lactate in the absence of glucose, with (grey) and without (blue) the monocarboxylate transporter (MCT) inhibitors 4-CIN (200 μ M) and AR-C155858 (1 μ M). The ability to sustain HFS EPSC trains was assessed at 10 and 30 minutes.

(A) 10 min: the raw EPSC amplitude during HFS was not significantly different following perfusion with lactate alone or lactate plus MCT inhibitors. Insets show EPSC amplitude for the first 0.1 s of HFS and example traces show the first 5 EPSCs of the HFS.

(B) 30 min: the raw EPSC amplitude during HFS was maintained with 10 mM lactate alone, but greatly reduced by addition of the MCT inhibitors with EPSC failures during the HFS in 1 of the 3 recordings.

Figure 8. Presynaptic terminals can utilise glucose or lactate to maintain synaptic transmission.

(A) Raw EPSC amplitudes and (B) mean normalised EPSC amplitudes plotted during HFS show that the magnitude of EPSC depression was similar after 30 min perfusion with either 1 mM glucose (grey) or 1 mM lactate (blue) alone. (A inset) Left plot shows the first 0.1 s of HFS. Right inset shows the experimental conditions. (B inset) Left plot shows the normalised EPSC amplitudes for the first 0.1 s of HFS.

Right plot shows example traces of the first 5 EPSCs of HFS using glucose or lactate as the sole presynaptic metabolic substrate.

(C) Raw EPSC amplitudes and (D) mean normalised EPSC amplitudes during HFS after 30 min of perfusion with 1 mM glucose alone (grey) and 1 mM glucose plus the monocarboxylate transporter (MCT) inhibitors (red; 4-CIN, 200 μ M + AR-C155858, 1 μ M). The MCT inhibitors significantly enhanced EPSC depression. (C inset) the left plot shows EPSC amplitudes for the first 0.1 s of HFS. The right inset shows the experimental conditions. (D inset) Left plot shows is the EPSC amplitudes for the first 0.1 s of HFS. Right plot shows example traces of the first 5 EPSC of HFS.

(E) EPSC amplitude fully recovers following HFS in the presence of 1 mM glucose, 1 mM lactate or 1 mM glucose plus MCT inhibitors, however see figure 9.

(F) Summary of the average EPSC amplitude during HFS. For each individual recording every 100th EPSC of HFS (i.e. 30 EPSCs in total) was averaged, these are the EPSCs used for statistical analysis (RM-ANOVA).

(G) Western blots show increased AMP kinase and phosphorylated AMP kinase (Thr172), in slices perfused with 1 mM glucose compared to 10 mM glucose. 1 mM glucose plus MCT inhibitors gave no further increase in AMPK or Thr172 pAMPK.

Figure 9. Analysis of individual recovery curves reveals that MCT inhibitors reduce the contribution of fast EPSC recovery in 1 mM glucose.

Individual recovery curves from single calyx of Held synapses (indicated by the different colours) from the 30 min HFS epoch while being perfused with one of three different substrate conditions.

(A & B) 1 mM glucose, (C) 1 mM glucose plus MCT inhibitors and (D) 1 mM lactate.

Data in black squares/lines in A-C show curves that could not be fit by a double exponential and have been excluded from subsequent analysis.

(E) Plot of percentage amplitude contribution by the fast recovery time constant; this was significantly reduced by MCT inhibitors. There was no difference between the 1 mM lactate and 1 mM glucose conditions.

(F) The value of the fast time constant of recovery was not significantly different between with the three conditions: 1 mM glucose, 1 mM glucose plus MCT inhibitors or 1 mM lactate.

(G) The value of the slow time constant of recovery was not significantly different between with the three conditions: 1 mM glucose, 1 mM glucose plus MCT inhibitors or 1 mM lactate.

Figure 10. Glycogenolysis makes no contribution to presynaptic metabolism in the presence of 1 mM extracellular glucose.

(A) Raw EPSC amplitudes and (B) normalised mean EPSC amplitudes during HFS show that after 30 min of perfusion with 1 mM glucose plus the glycogenolysis inhibitor (black; DAB, 500 μ M) there was no difference in EPSC depression compared to with 1 mM glucose alone (grey). Insets show the first 0.1 s of HFS and example EPSC traces show the first 5 EPSCs of HFS.

(C) The addition of DAB in the presence of 1 mM of glucose had no effect on the EPSC recovery curve.

(D) Summary showing the average EPSC amplitude during the 30 s of HFS was similar in the presence or absence of DAB.

Figure 11. Glycogenolysis can contribute to maintenance of synaptic transmission during washout of glucose.

(A) Raw EPSC amplitudes and (B) normalised mean EPSC amplitudes during HFS , show that after 15 min of perfusion with 0 mM glucose plus MCT inhibitors (red; 200 μ M 4-CIN + 1 μ M AR-C155858) or 0 mM glucose plus the glycogenolysis inhibitor (black; 500 μ M DAB) there was increased EPSC depression compared to with 0 mM glucose alone (grey). Insets show the first 0.1 s of HFS and example EPSC traces give the first 5 EPSCs of HFS.

(C) The addition of the MCT inhibitors or DAB in the absence of glucose did not change the recovery.

(D) Summary of the average EPSC amplitude during the 30 s of HFS at 15 minutes exposure show that both MCT inhibitors and DAB cause a significant reduction in EPSC amplitude.

(E) Delivery of HFS epochs was continued beyond 15 minutes and the number of stimuli delivered (3000 per HFS train) before observation of the first transmission failure is reduced in the presence of DAB.

Figure 12. Summary diagram showing the route of metabolic substrate utilisation by the presynaptic terminal and the effects of ATP depletion on transmitter release.

Under physiological conditions the presynaptic terminal will use glucose directly, and could also utilise local lactate made by glial cells. During glucose deprivation some energy is supplied in the form of the lactate from glycogen breakdown in the glial

cells. ATP depletion did not primarily effect vesicle release probability, but slowed vesicle replenishment and reduced the number of release sites possessing releasable vesicles, a reduction in endocytosis and vesicle recycling rates may also contribute to compromised transmission.

Table 1

	Control				Zero glucose			
	10 min	15 min	20 min	25 min	10 min	15 min	20 min	25 min
τ_{r0} (s)	0.042	0.039	0.044	0.042	0.045	0.040	0.051	0.063
τ_f (s)	0.010	0.021	0.010	0.010	0.010	0.035	0.056	0.019
P_o	0.163	0.178	0.128	0.131	0.133	0.192	0.176	0.199
k_f (fixed)	0.030	0.030	0.030	0.030	0.030	0.030	0.030	0.030
A_n	0.440	0.412	0.454	0.417	0.538	0.264	0.085	0.045
τ_n (s)	10.978	9.712	11.844	10.570	11.709	12.068	13.115	8.674
k_n	6.318	7.014	5.428	6.187	2.699	8.500	3.890	2.571
τ_l (s)	2.089	2.546	2.906	2.318	3.342	0.813	12.175	3.696
k_i	0.0023	0.0017	0.0015	0.0017	0.0018	0.0033	0.0026	0.0026
τ_{rR} (s)	2.907	2.821	2.755	1.952	6.674	1.499	2.187	3.608
τ_{rD} (s)	2.546	1.621	1.194	1.351	0.707	1.216	0.747	1.149
$nRec$	0.828	0.875	0.920	0.877	1.085	0.653	0.634	0.063

Table 1. Model parameter values.

Model parameter values obtained from fitting to the mean data in 10 mM glucose and zero glucose for each HFS epoch (as indicated at 10, 15, 20 and 25 min).

1128 **Additional Information**

1129

1130 The authors declare no competing interests.

1131 All authors have approved the final version of the MS and agree to be accountable
1132 for the work. Only authors that qualify for authorship have been listed.

1133

1134 Funding is stated on Page 1

1135

1136 **Author Contributions:**

1137 SL: Expt design, electrophysiology and imaging acquisition and analysis, MS drafting
1138 and revision.

1139 CBM: Modelling, analysis, MS drafting.

1140 VM: Expt design, analysis, MS drafting.

1141 JLS: Western blot acquisition and analysis, MS drafting.

1142 MHH: Expt and modelling design and interpretation, MS drafting and revision.

1143 BG: Expt and modelling design and interpretation, MS drafting and revision.

1144 IDF: Expt Design, interpretation, MS drafting and revision.

Figure 1

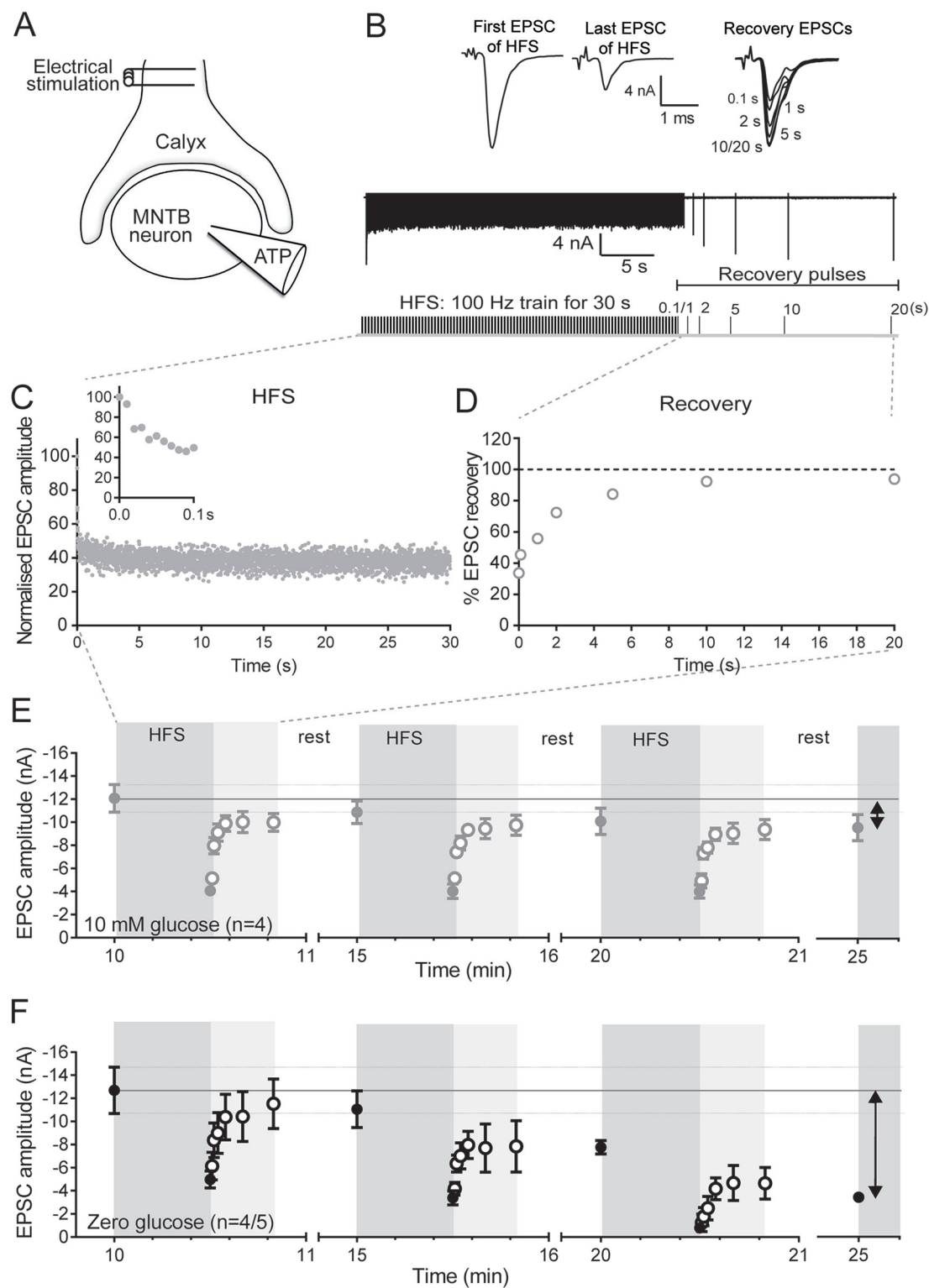


Figure 2

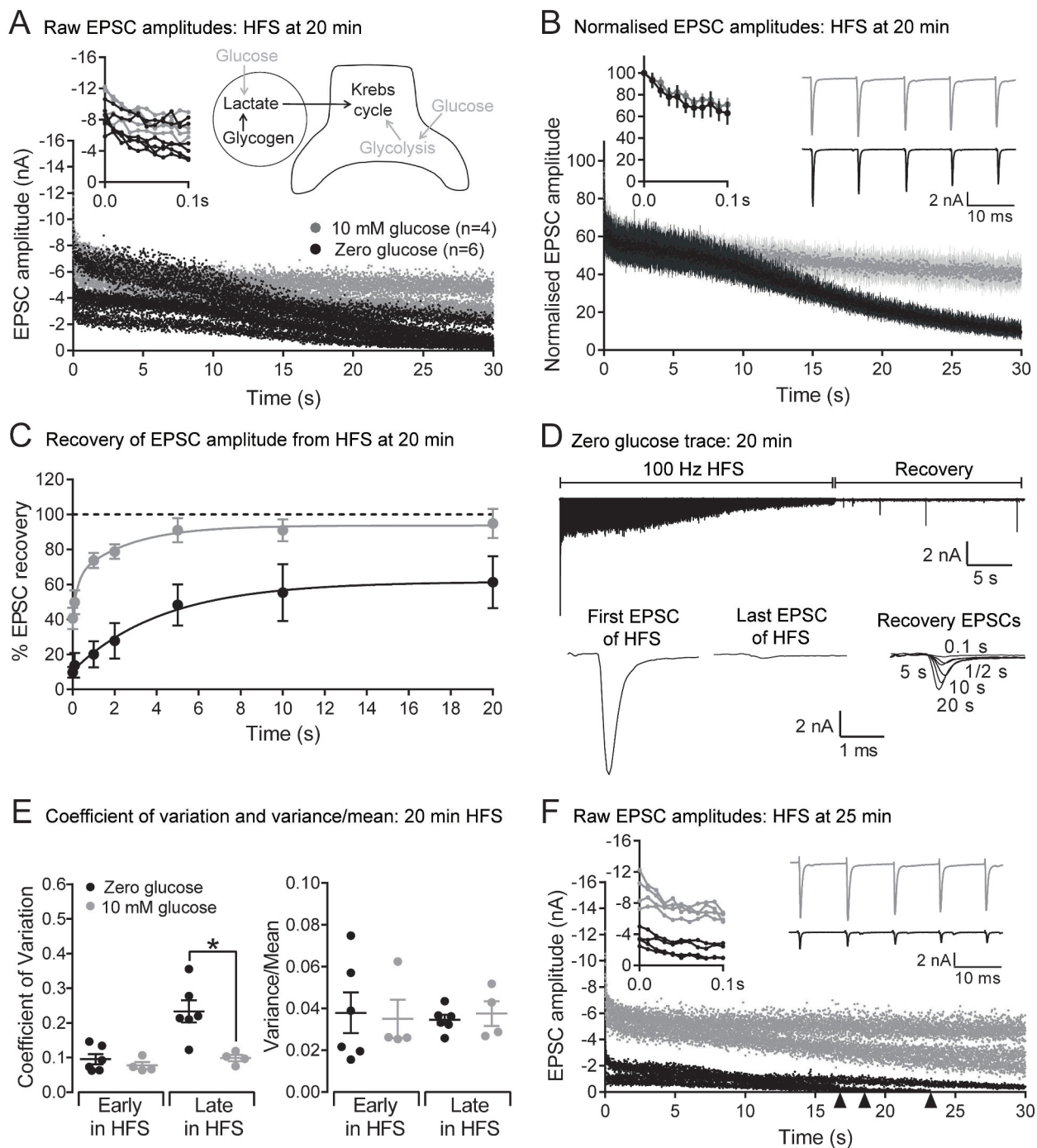


Figure 3

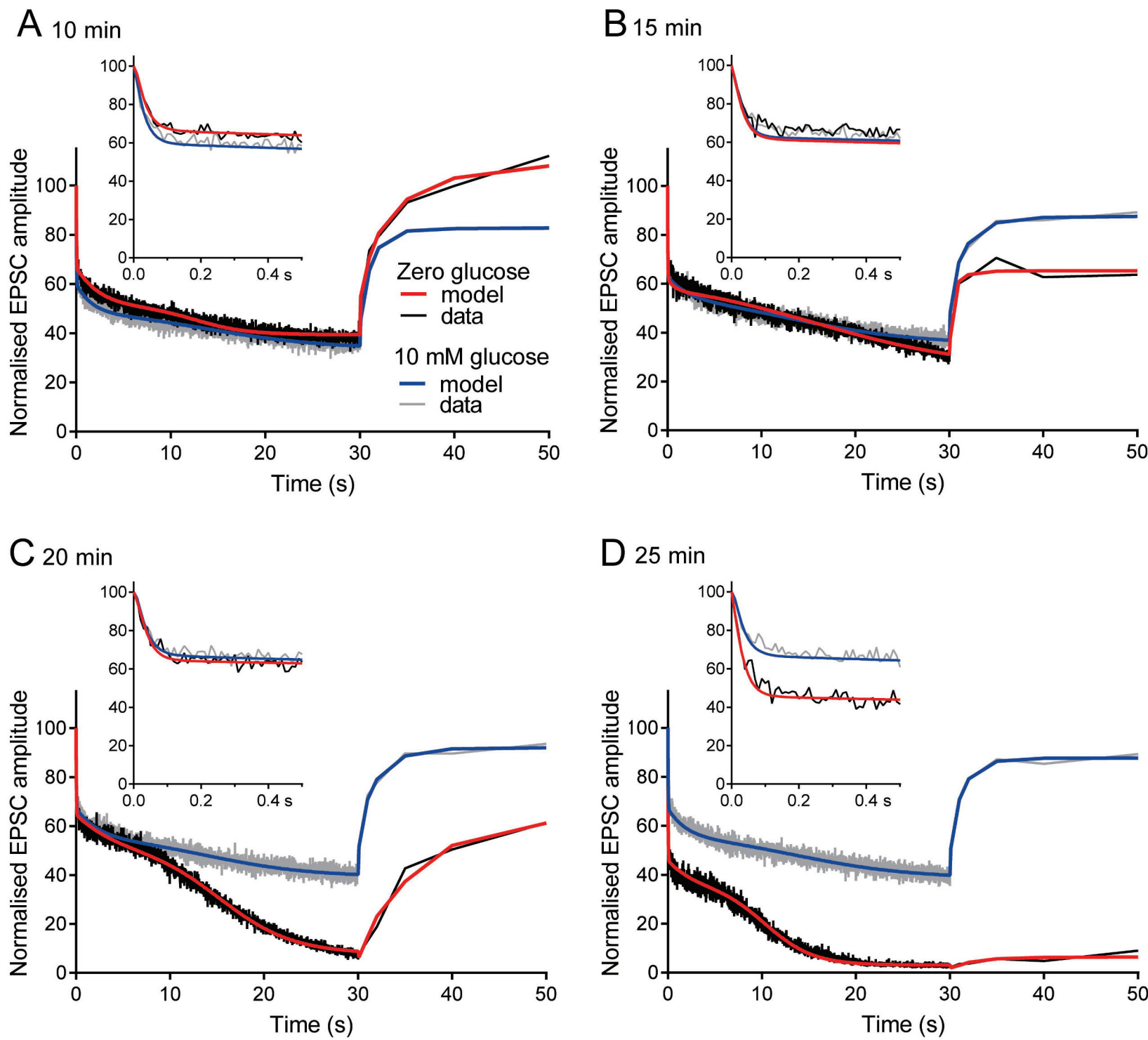
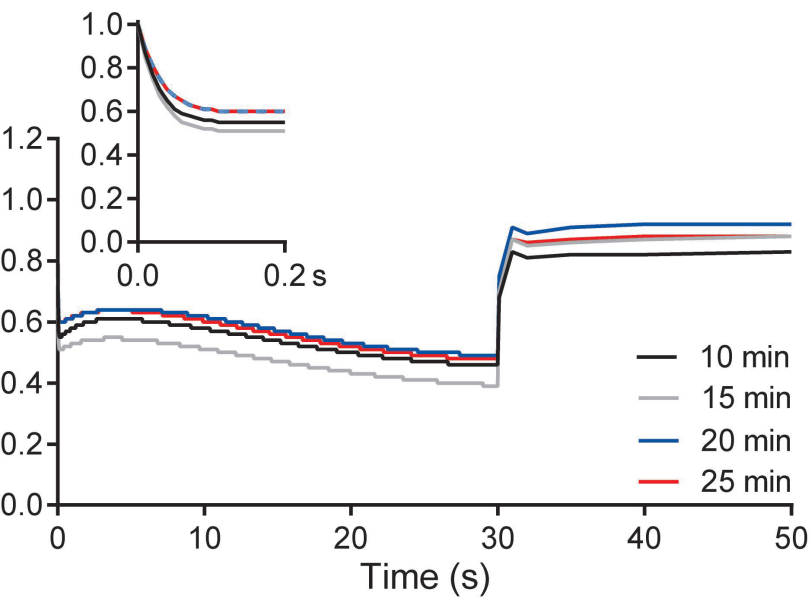
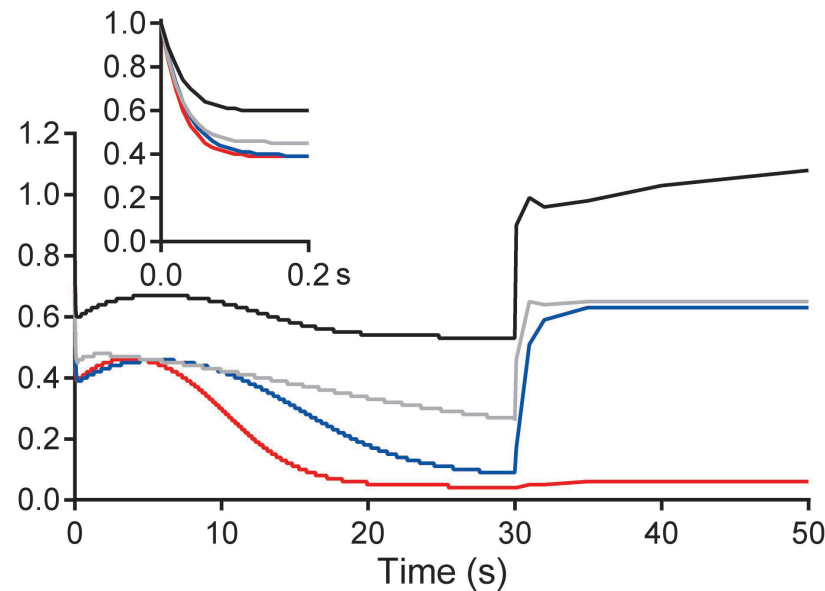


Figure 4

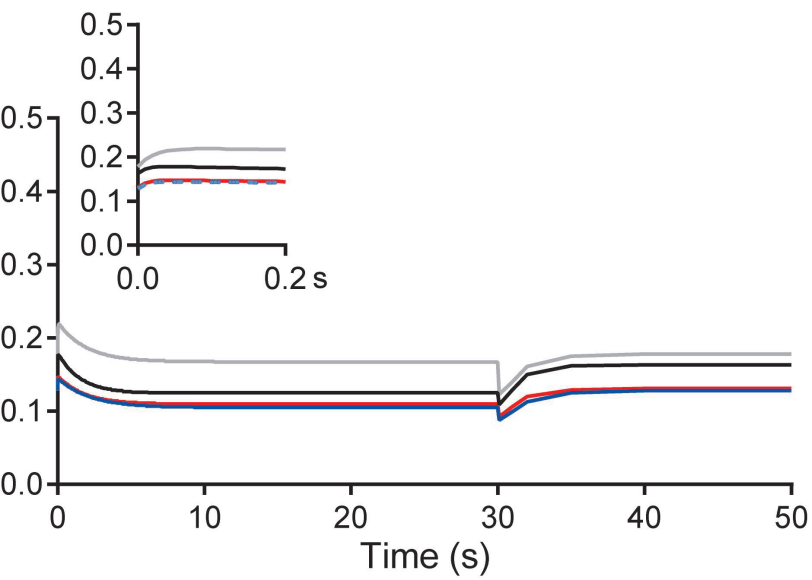
A n: 10 mM glucose



B n: zero glucose



C p: 10 mM glucose



D p: zero glucose

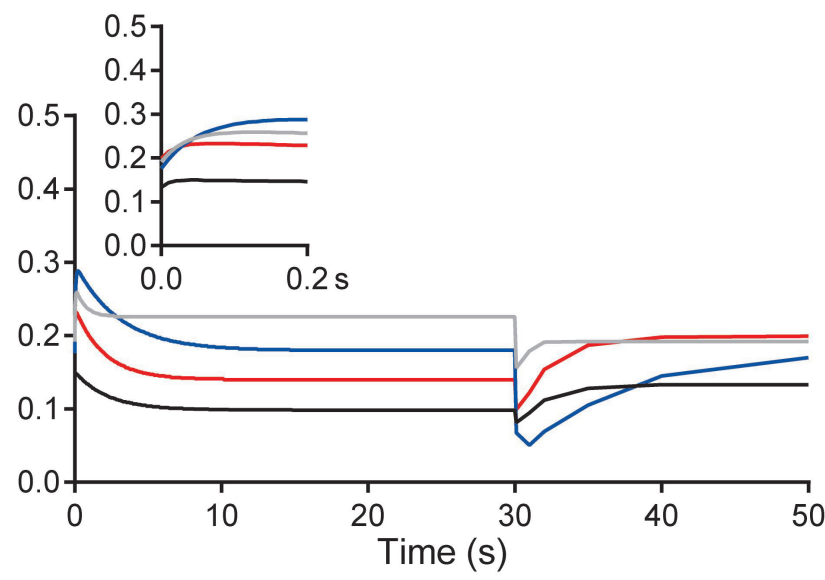


Figure 5

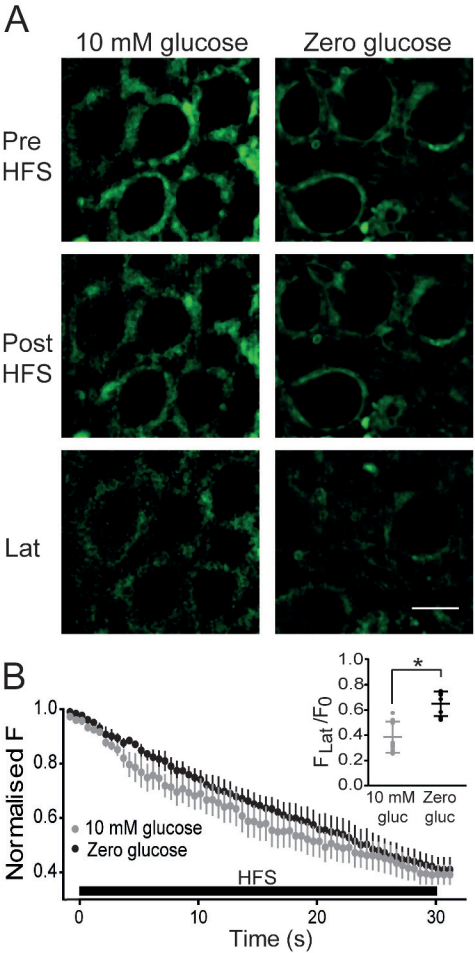


Figure 6

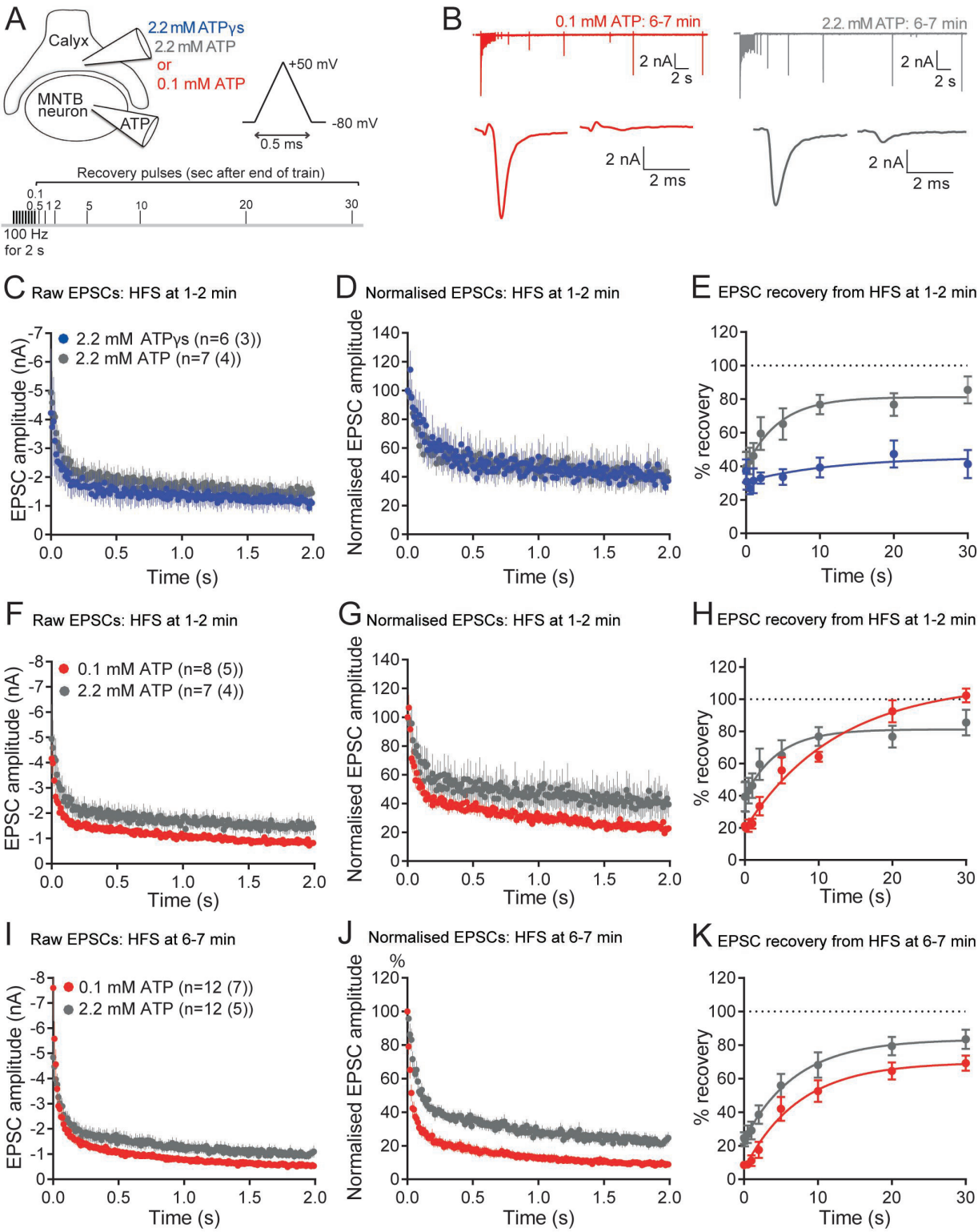


Figure 7

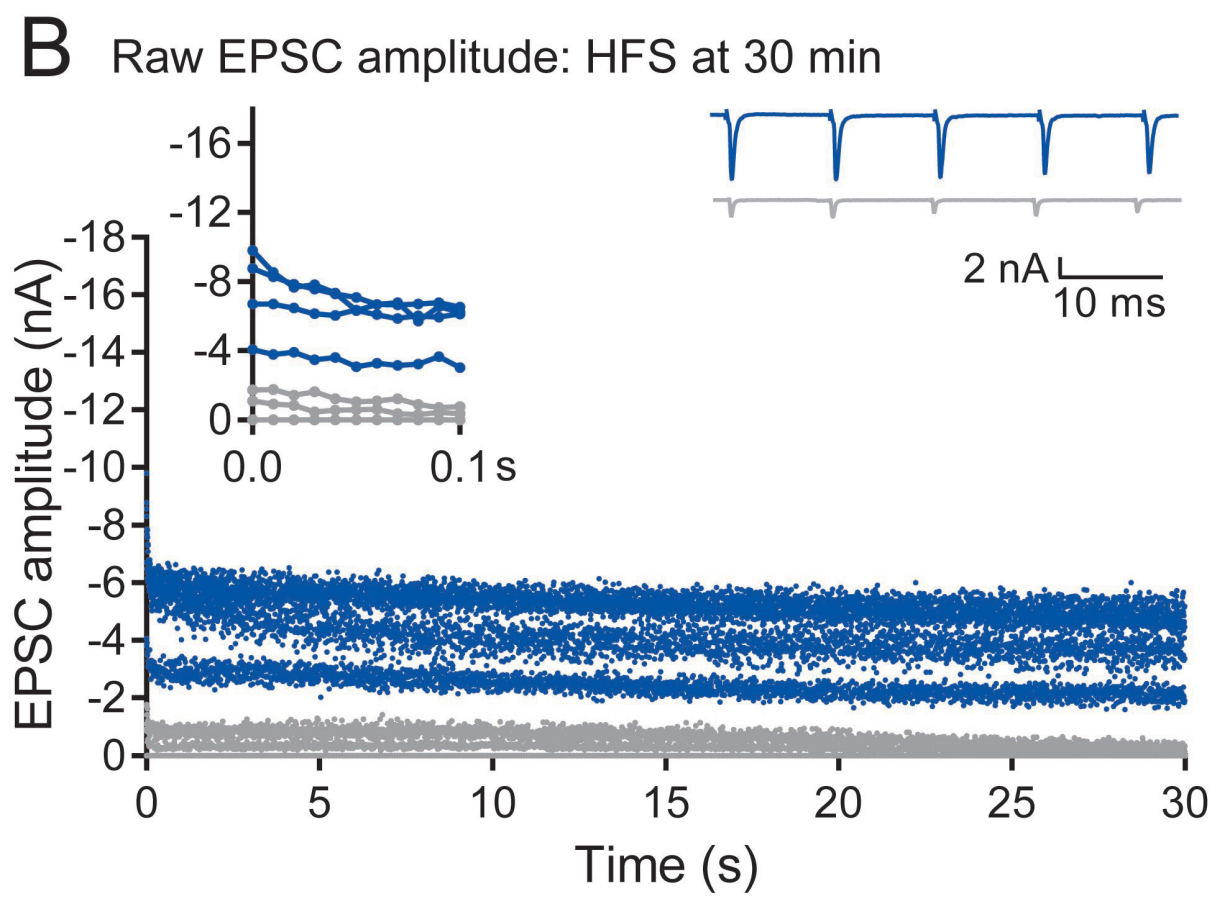
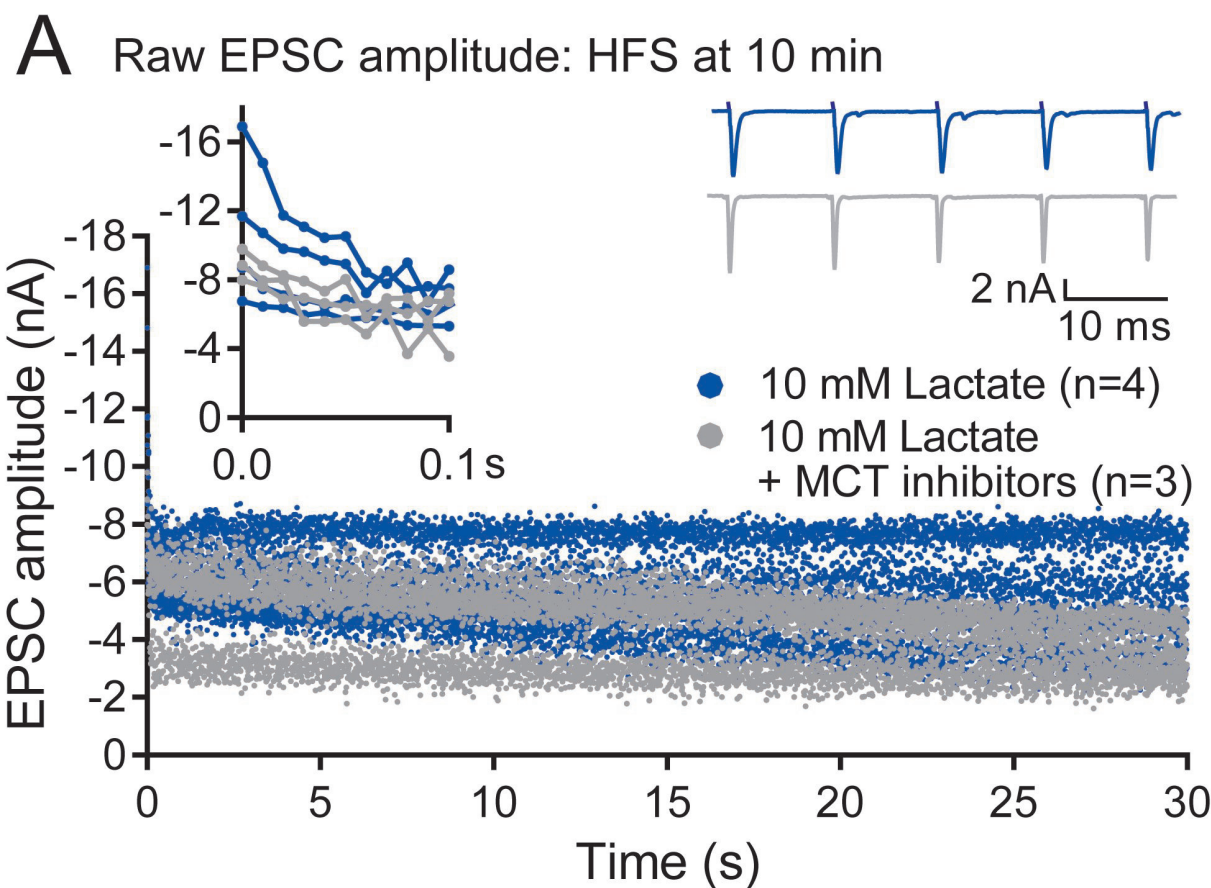


Figure 8

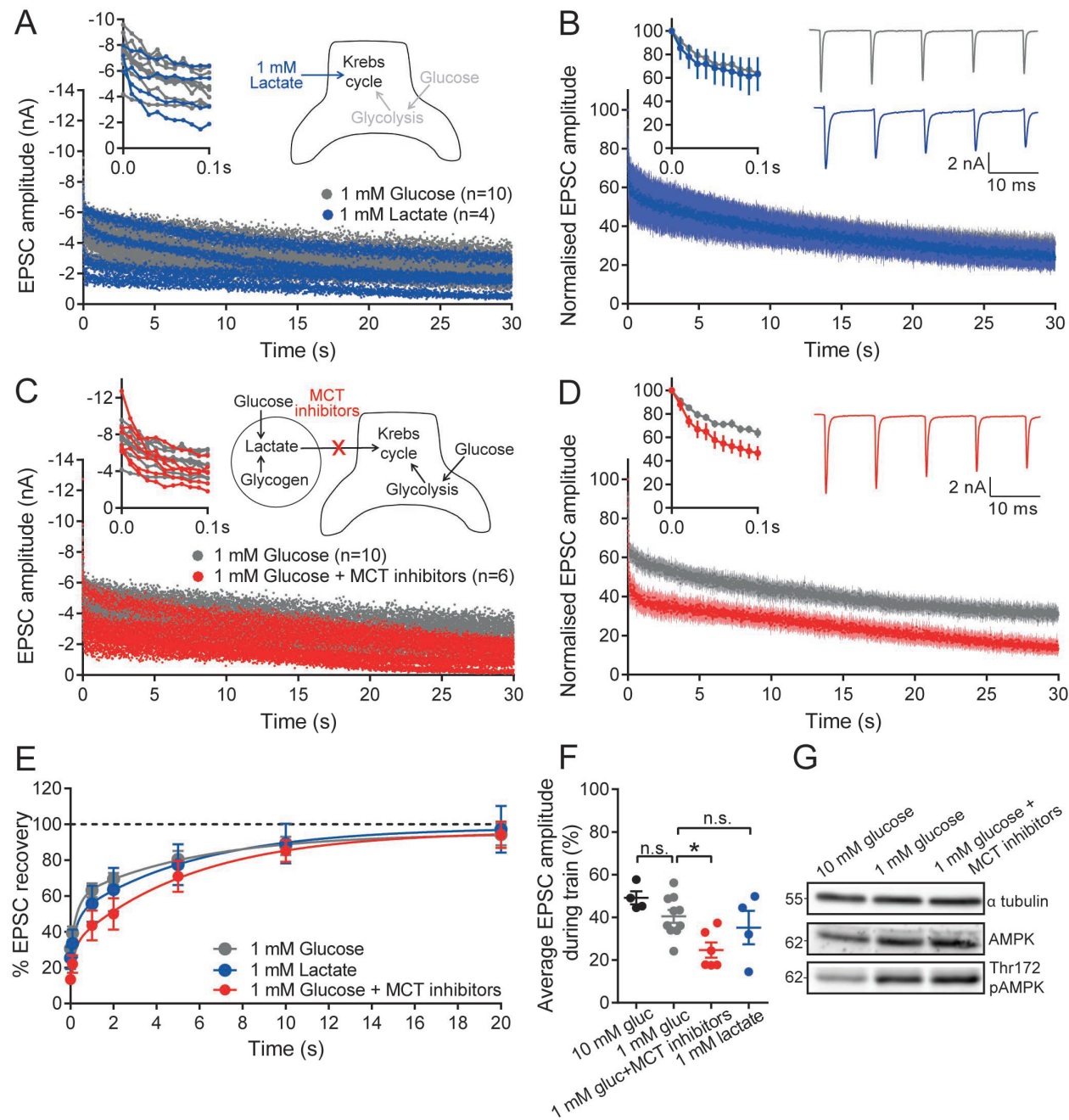


Figure 9

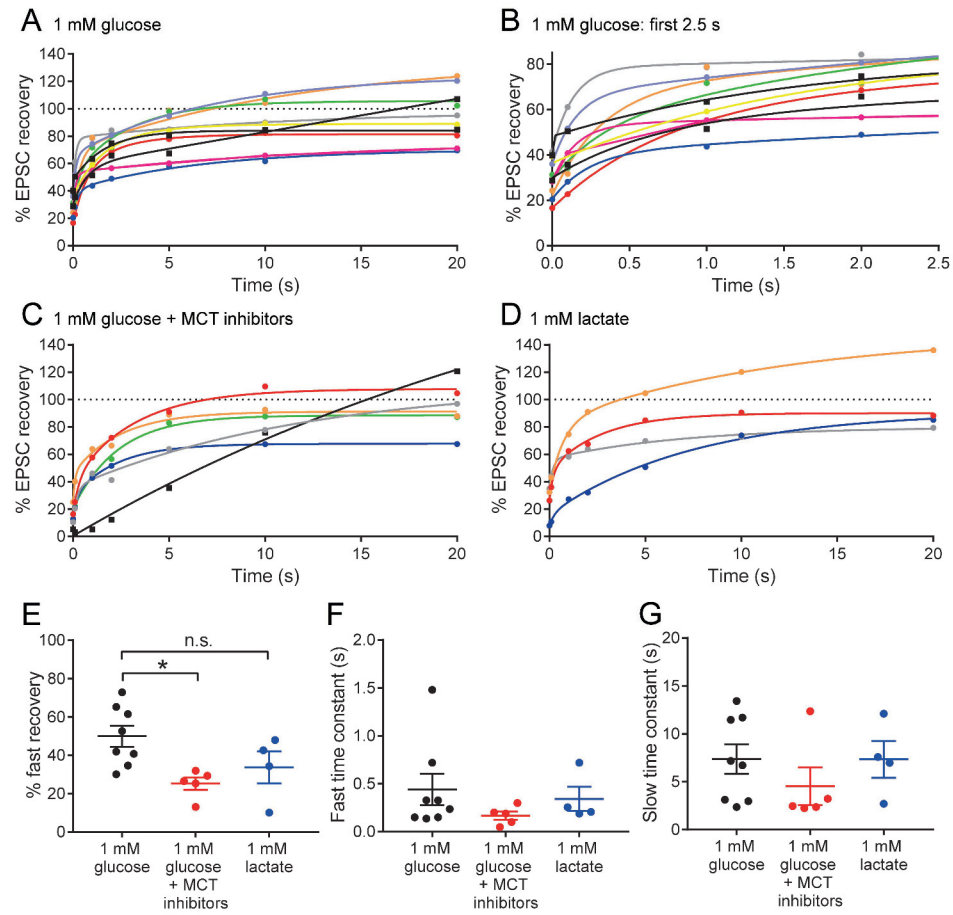


Figure 10

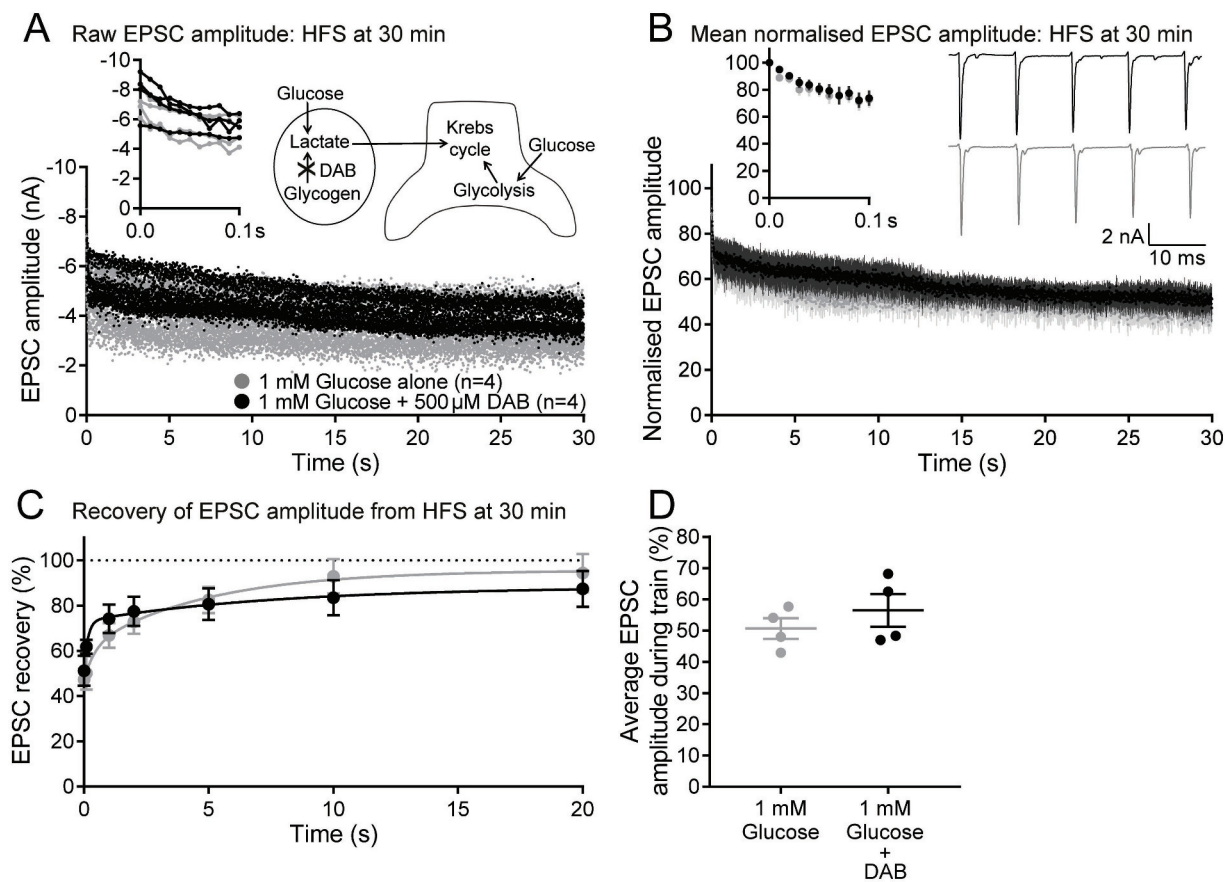
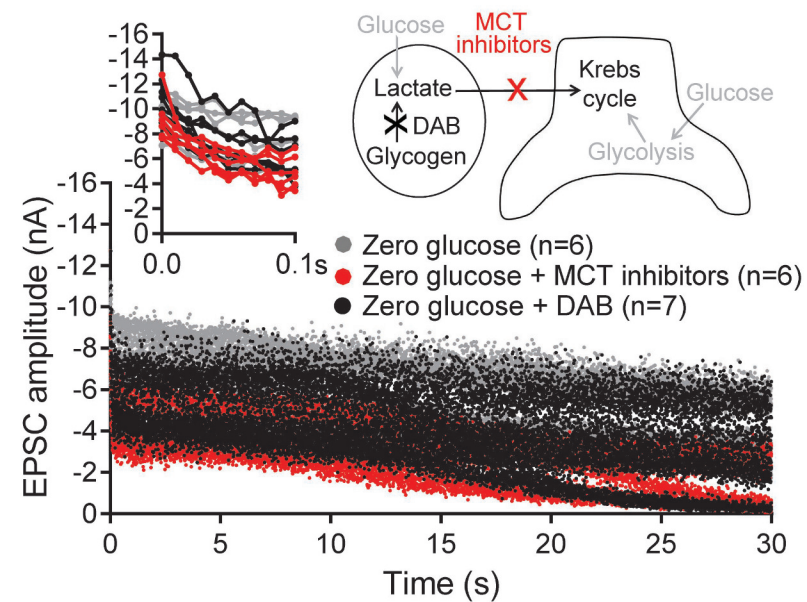
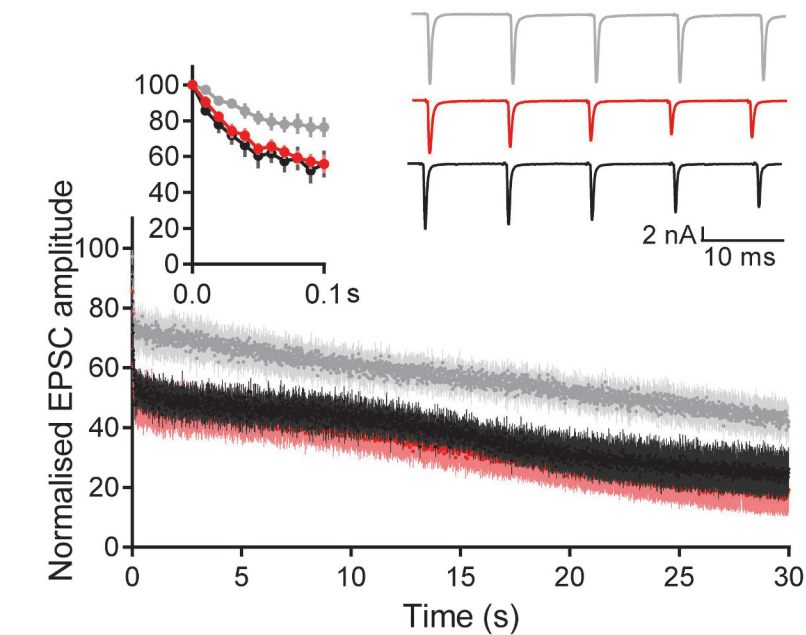


Figure 11

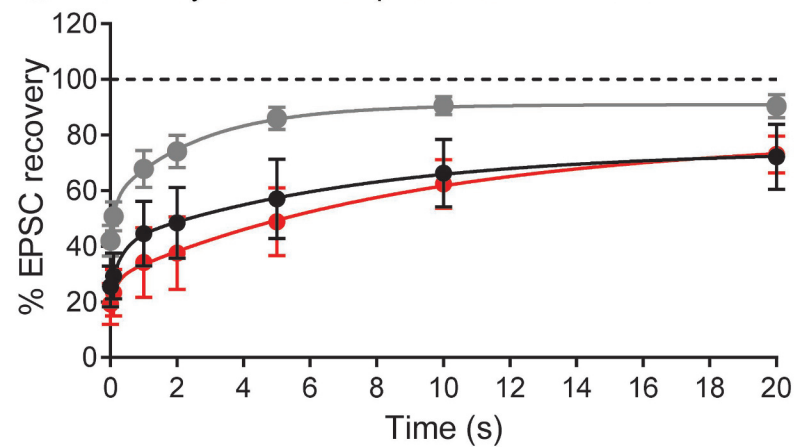
A Raw EPSC amplitude: HFS at 15 min



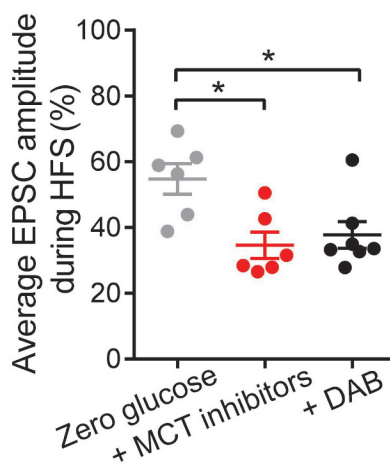
B Mean normalised EPSC amplitude: HFS at 15 min



C Recovery of EPSC amplitude from HFS at 15 min



D



E

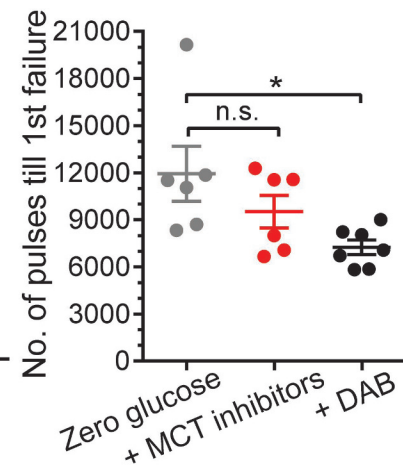


Figure 12

